Long-term labeling and imaging of synaptically-connected neuronal networks *in vivo* using nontoxic, double-deletion-mutant rabies viruses

Lei Jin[1], Heather A. Sullivan[1], Mulangma Zhu[1], Thomas K. Lavin[1], Makoto Matsuyama[1], Nicholas E. Lea[1], Ran Xu[1], YuanYuan Hou[1], Luca Rutigliani[1], Maxwell Pruner[1], Kelsey R. Babcock[1], Jacque Pak Kan Ip[2,3,4], Ming Hu[2,3,5], Tanya L. Daigle[6], Hongkui Zeng[6], Mriganka Sur[2,3], & Ian R. Wickersham[1]*

1. McGovern Institute for Brain Research, Massachusetts Institute of Technology, Cambridge, MA, USA
2. Department of Brain and Cognitive Sciences, Massachusetts Institute of Technology, Cambridge, MA, USA
3. Picower Institute for Learning and Memory, Massachusetts Institute of Technology, Cambridge, MA, USA
4. School of Biomedical Sciences, The Chinese University of Hong Kong, Hong Kong, China
5. Department of Neuroscience, Baylor College of Medicine, Houston, TX, USA
6. Allen Institute for Brain Science, Seattle, WA, USA
*Corresponding author (wickersham@mit.edu).

Summary
The highly specific and complex connectivity between neurons is the hallmark of nervous systems, but techniques for identifying, imaging, and manipulating synaptically-connected networks of neurons are limited. Monosynaptic tracing, or the gated replication and spread of a deletion-mutant rabies virus to label neurons directly connected to a targeted population of starting neurons[1], is the most widely-used technique for mapping neural circuitry, but the rapid cytotoxicity of first-generation rabies viral vectors has restricted its use almost entirely to anatomical applications. We recently introduced double-deletion-mutant second-generation rabies viral vectors, showing that they have little or no detectable toxicity and are efficient means of retrogradely targeting neurons projecting to an injection site[2], but they have not previously been shown to be capable of gated replication *in vivo*, the basis of monosynaptic tracing. Here we present a complete second-generation system for labeling direct inputs to genetically-targeted neuronal populations with minimal toxicity, using double-deletion-mutant rabies viruses. Spread of the viruses requires complementation of both of the deleted viral genes *in trans* in the starting postsynaptic cells; suppressing the expression of these viral genes following an initial period of viral replication, using the Tet-Off system, reduces toxicity to the starting cells without decreasing the efficiency of viral spread. Using longitudinal two-photon imaging of live monosynaptic tracing in visual cortex, we found that 94.4% of all labeled cells, and an estimated 92.3% of starting cells, survived for the full twelve-week course of imaging. Two-photon imaging of calcium responses in labeled networks of neurons *in vivo* over ten weeks showed that labeled neurons' visual response properties remained stable for as long as we followed them. This nontoxic labeling of inputs to genetically-targeted neurons *in vivo* is a long-held goal in neuroscience, with transformative applications including nonperturbative transcriptomic and epigenomic profiling, long-term functional imaging and behavioral studies, and optogenetic and chemogenetic manipulation of synaptically-connected neuronal networks over the lifetimes of experimental animals.

Introduction
Monosynaptic tracing, or the labeling of neurons in direct synaptic contact with a targeted neuronal population using a deletion-mutant neurotropic virus, has become an important technique in neuroscience since its introduction in 2007[1], because it is the primary available means of brain-wide identification of directly connected neurons. Its core principles are (i) the selective infection of a targeted neuronal group of interest with a deletion-mutant neurotropic virus (which in almost all implementations

to date is a rabies virus with the envelope glycoprotein gene "G" deleted from its genome) and (ii) the complementation of the deletion *in trans* in the targeted starting cells, so that the virus can fully replicate within them and spread, as wild-type rabies virus does, retrogradely (in the CNS[3]) across those neurons' input synapses to the neurons directly presynaptic to them. This system has contributed to many significant discoveries about the synaptic organization of many systems in the mammalian nervous system[4-16].

However, with a few notable exceptions[4,7,17-21], monosynaptic tracing has primarily served simply as an anatomical tool for static identification of connected neurons, because the first-generation, "ΔG" rabies viral vectors that it is based on are swiftly cytotoxic[2,22,23]. This toxicity stems from the fact that, while deletion of the glycoprotein gene, as intended, prevents the virus from spreading between neurons in the absence of transcomplementation, it leaves the viral transcription and replication machinery intact, so that the virus still rapidly expresses viral genes at high levels and replicates the viral core to high copy numbers[24], perturbing endogenous gene expression[25,26], inhibiting host cell protein synthesis[27], and killing most infected neurons within approximately two weeks[2,22].

Several efforts have been made to engineer less-toxic or nontoxic monosynaptic tracing systems. A first-generation system based on the CVS-N2c strain of rabies virus appears to have lower toxicity than does the widely-used SAD B19 strain[23]; however, there is no claim or indication that CVS-N2c vectors are completely nontoxic to either postsynaptic or presynaptic cells. More recently, a paper in *Cell* reported that adding a destabilization domain to the C terminus of the viral nucleoprotein rendered the virus nontoxic, allowing monosynaptic tracing "with no adverse effects on neural physiology, circuit function, and circuit-dependent computations"[28]; however, we have since shown that those results were almost certainly obtained using reversion mutants that had lost the intended C-terminal addition[29,30]. In our own laboratory, we introduced second-generation, "ΔGL" rabies viral vectors, which have the viral polymerase gene "L" (for "large" protein) deleted along with G, and showed that they do not perturb the structure or function of labeled neurons; however, we have not previously shown that they can spread between neurons[2].

Here we show that the nontoxic second-generation (ΔGL) rabies viral vectors can be used for monosynaptic tracing of inputs to genetically-defined populations of neurons, with the double deletion complemented by expression of both deleted viral genes *in trans* in the starting cells. Using two-photon microscopy for structural imaging of labeled networks of neurons in visual cortex over twelve weeks, we found that the great majority of even the starting postsynaptic cells (in which the virus is allowed to replicate by complementation of its two deleted genes) survived for as long as we imaged them. Using two-photon functional calcium imaging of labeled visual cortical cells, we found that their visual responses to drifting gratings remained stable over the full ten-week course of imaging.

Construction of a monosynaptic tracing system based on ΔGL rabies viruses

Because we planned for the second-generation monosynaptic tracing system to use the same pseudotyping strategy[1] used in the first-generation one for targeting the initial RV infection to the postsynaptic "starting cells", we began by making versions of our previously-introduced second-generation (ΔGL) rabies viral vectors[2] packaged with the ASLV-A envelope protein EnvA, for selective infection of cells engineered to express EnvA's receptor, TVA[31,32].

Whereas the first-generation system typically relies on an AAV "helper virus" for expression of the deleted glycoprotein gene *in trans* in the starting cells[33-36], the polymerase gene that is also deleted in the second-generation vectors is ~6.4 kb, too large[37-40] for a straightforward extension of this approach. We also wanted expression of both the polymerase and the glycoprotein to be regulatable using the tetracycline system[41], because we anticipated that sustained expression and concomitant viral replication could be cytotoxic to starting cells.

We therefore generated a knock-in mouse line, "TRE-CB" (short for "TRE-tight-mCardinal-P2A-B19L"), in which the genes for the RV polymerase (SAD B19 strain) and the red fluorophore mCardinal[42] are under the control of the tetracycline response element in the TIGRE locus[43-45]. To interface with this TRE-driven polymerase allele, we developed a helper virus combination (now published for use with first-generation RV[36,46,47]) based on the tet system. Specifically, one AAV, "AAV1-syn-FLEX-splitTVA-EGFP-tTA" is Cre-dependent[48] (FLEX/DIO design[49]) and expresses TVA, EGFP[50,51], and the tet transactivator (tTA), while a second AAV, "AAV1-TREtight-mTagBFP2-B19G", expresses the RV glycoprotein and the blue fluorophore mTagBFP2[52] under the control of the tet response element. Our intent was, when the helper viruses were used in the TRE-CB mouse with Cre expression in starting cells, that the tTA

expressed by the first AAV would drive expression both of G from the second AAV and of L from the knock-in allele. Note that the use of tTA instead of rtTA makes this a Tet-Off system, so that the genes are expressed by default, with optional administration of a tetracycline analog (specifically, doxycycline) serving to suppress their expression.

Because ΔGL viruses, by design, express genes at very low levels and are therefore designed to express recombinases, both for signal amplification and versatility of downstream applications[2], the virus in this case expressed Flpo, a codon-optimized version of the yeast recombinase[53,54]. The last necessary component of the system was therefore a means of reporting Flp activity, for which we used the "Ai65F" mouse line[45], in which recombination causes tdTomato expression in Flp-expressing cells. In this implementation, therefore, the system requires triple-transgenic mice, with a Cre line crossed to the TRE-CB and Ai65F lines (the breeding for this, however, can be quite simple; see Discussion).

Based on our extensive prior experiments titrating these helper viruses for use with first-generation rabies virus to achieve high transsynaptic spread efficiency in Cre mice but low background without Cre[46,47], for this second-generation system we used the same helper virus concentrations and seven-day interval between AAV and RV injections as we have previously described for the first-generation one, only varying the survival time after RV injection.

Mapping inputs to dopaminergic and parvalbumin-expressing neurons in Cre mouse lines

We tested the system in two widely-used Cre mouse lines: DAT-IRES-Cre[55] and PV-Cre[56] (crossed to TRE-CB and Ai65F)(Fig. 1 and Extended Data Figs. 2 & 3). In DAT-IRES-Cre, in which Cre is expressed in dopaminergic cells in the midbrain, we injected the viruses in substantia nigra, pars compacta (SNc); in PV-Cre, in which Cre is expressed in parvalbumin-expressing cells in cortex and other brain regions, we injected primary somatosensory cortex (S1). In order to test the effect of using the Tet-Off mechanism to suppress G and L expression after an initial period of unrestricted viral replication, half of the mice were switched to doxycycline-containing food two weeks after rabies virus injection.

In both mouse lines, with or without doxycycline, we found significant spread of rabies virus to regions known to provide input to the respective populations: in DAT-IRES-Cre, we found labeled neurons in striatum (Fig. 1b) and cortex; in PV-Cre, we found labeled neurons in thalamus (Fig. 1e) and other cortical areas, among other locations. In both mouse lines, there were more neurons at a later time point (five weeks following rabies virus injection) than at an earlier one (three weeks) (see Supplementary Files 1 and 2 for all cell counts and statistical comparisons) (because pilot studies had suggested that survival times of one or two weeks did not result in substantial spread, and survival times of seven weeks and higher did not result in much more spread than at five weeks, we only compared three- and five-week survival times for this set of quantitative experiments). This spread of the ΔGL virus to input regions, increasing with time, was despite the fact that we were unable to see clear mCardinal signal, suggesting very low expression of L under the conditions implemented (Extended Data Fig. 1).

Crucially, control experiments in which either Cre or G was omitted resulted in almost no labeled cells in input regions (Fig. 1 & Extended Data Figs. 2 & 3). This indicates that the apparent transsynaptic spread was not due to trivial confounding effects (such as direct retrograde infection by the TVA-expressing helper AAV followed by infection of the resulting TVA-expressing axons by the rabies virus, or simply direct retrograde infection by residual RV coated with its native glycoprotein. For more discussion of such possible confounds, see Lavin et al.[46]).

Also importantly, control experiments in which L was omitted (by using double transgenics without the TRE-CB allele) also resulted in no label in input regions. This indicates that, as expected, complementation with both G and L is required for the ΔGL virus to replicate within the starting cells and spread to presynaptic ones.

A somewhat surprising result from these experiments was that doxycycline administration beginning two weeks after rabies virus injection appeared to modestly *increase* (although not statistically significantly) transsynaptic spread in both mouse lines and at both survival times. This was contrary to our expectation that this intervention, which was designed to reduce toxicity to starting cells by shutting off viral replication after an initial period, could also reduce the efficiency of transsynaptic spread.

Comparison to the first-generation system in the same Cre lines, however, showed that this implementation of the second-generation one appeared to be far less efficient: matched experiments using a first-generation virus, RVΔG-Flpo (and in mice without the TRE-CB allele), labeled 1.3-1.5 orders of magnitude (~21x in DAT-IRES-Cre, ~33x in PV-Cre) more neurons in input regions (Fig. 1c & 1f).

Labeling inputs to corticostriatal projection neurons: Cre vs Flpo

We hypothesized that the apparent low efficiency of the second-generation system could be partially due simply to Flpo itself being inefficient[54,57]: because ΔGL viruses, by design, express at low levels, their expression of a relatively ineffectual recombinase could be insufficient to recombine the Ai65F reporter allele in some cells, potentially masking a much higher actual efficiency of viral spread. We therefore conducted a set of experiments to compare the effect of using Cre, as opposed to Flpo, as the transgene expressed by the ΔGL virus.

We designed an experiment to test the effect of switching the recombinases' roles, so that Cre would be expressed by the rabies virus and Flpo would be used to select the starting cell population. We targeted corticostriatal cells in primary somatosensory cortex (S1) using retrograde infection by rAAV2-retro[58] injected in dorsolateral striatum (Fig. 2), with helper AAVs and subsequently RVΔGL injected into S1. In one design (Fig. 2a), the rAAV2-retro expressed Cre, the helper AAVs were the same Cre-dependent ones as used above, and the RVΔGL was the same Flpo-expressing version; these injections were done in the same Ai65F reporter line used above (crossed to TRE-CB). In the other design (Fig. 2b), the rAAV2-retro expressed Flpo, the helper AAVs were Flpo-dependent (i.e., the first helper virus contained orthogonal FRT sites instead of lox sites), and the RVΔGL expressed Cre instead of Flpo; these injections were done in the Cre-dependent tdTomato-expressing reporter line Ai14[59] (crossed to TRE-CB). Titers of AAV and RV vectors were matched across the two designs (see Methods). Two to five weeks after rabies virus injection, mice were perfused and the results examined by confocal microscopy, with transsynaptic spread efficiency quantified by counting labeled neurons in contralateral cortex and ipsilateral thalamus.

Due to an error in the principal investigator's design of the Flp-dependent helper AAV, this virus contained an in-frame stop codon within the FRT site at the beginning of the TVA950 gene, so that TVA was presumably not expressed. Despite this, the experiments were very successful, as described below, with the only indication of irregularity being the long time needed for spread of the first-generation virus (12 days, as opposed to the 7 days our laboratory typically uses). EGFP (from the same helper virus) and mTagBFP2 (from the second helper virus, which depends for its expression on the tTA from the first helper virus) were both found to be expressed in the corticostriatal cells as intended (see below), presumably due to translation initiation (on transcripts from successfully Flpo-recombined AAV genomes) at one or both of the start codons that precede these two genes after the P2A sequences within the intended tricistronic open reading frame. We therefore attribute the undeserved success of these experiments to infection of the resulting G- and L-expressing corticostriatal neurons by residual RV virions coated with its native glycoprotein (mentioned above), followed by spread between the G-expressing corticostriatal cells and to the cells' inputs, as intended.

The results of the control experiments for both designs were very similar to those obtained using the Cre lines: omission of any of G, L, or Cre (in this case by leaving out the rAAV2-retro) resulted in almost no labeled cells in either contralateral cortex (Fig. 2e, left) or thalamus (Fig. 2e, right) (see also Extended Data Fig. 4, and see Supplementary File 3 for all counts and statistical comparisons).

The results using the Flpo-expressing RVΔGL when all components were included were also similar to those obtained in the Cre lines: we found modest numbers of labeled neurons in the input regions at two different survival times (2 and 5 weeks after RV injection), and again doxycycline administration seemed to slightly increase spread, though not significantly (see Supplementary File 3 for all cell counts and statistical comparisons). The first-generation version (using RVΔG-Flpo) still labeled significantly (in most cases) more cells in both input regions than any condition of the second-generation one did.

However, the second-generation system using the RVΔGL expressing Cre instead of Flpo was much more efficient. Similar to the other experiments, omission of G, L, or Flpo (again by omitting the rAAV2-retro) resulted in almost no label in input regions (Fig. 2f and Extended Data Fig. 4). With all components included, however, in both thalamus and contralateral cortex, the numbers of cells were actually greater with the second-generation virus than with the first-generation version (using RVΔG-Cre in this case), although these differences were not statistically significant (see Supplementary File 3 for counts and statistical comparisons). To an extent, the favorability of this comparison was due to a reduction in efficiency of the first-generation system (which in turn was almost certainly due to the misdesigned Flp-dependent helper virus): we got little spread of the RVΔG-Cre with a 7-day survival time, so we also included a 12-day time point, at which the numbers of labeled neurons were much higher but still considerably (85% for contralateral cortex, 65% for thalamus) lower than using RVΔG-Flpo with the Cre

dependent helpers. Even so, in absolute terms, the numbers of labeled neurons were much higher for RVΔGL-Cre than for RVΔGL-Flpo, ranging from 1.3x to 10.8x higher depending on the input region, survival time, and dox regimen (Supplementary File 3). The ratios of the numbers of labeled cells in contralateral cortex or thalamus to the numbers of starting cells were also higher for RVΔGL-Cre than for RVΔGL-Flpo (Supplementary Fig. 5).

Longitudinal two-photon imaging of labeled networks

We next conducted several experiments to determine how toxic the second-generation monosynaptic tracing system was to labeled neurons. We previously used longitudinal two-photon microscopy to show that neurons labeled with a second-generation (ΔGL) RV stayed alive for as long as we imaged them (in stark contrast to neurons labeled with a first-generation (ΔG) RV) and also that it did not perturb their visual response properties to any degree that we were able to detect[2]. Because we had only used the Cre-expressing versions of ΔG and ΔGL viruses for the longitudinal two-photon imaging work from our previous publications[2,29,30], for the two-photon work in the present paper we began by conducting a similar set of experiments using the Flpo-expressing version to confirm that it too was nontoxic (Extended Data Fig. 6). We found that it was: in contrast to the first-generation version, RVΔG-Flpo, which killed almost all labeled neurons by 4 weeks postinjection, the second-generation RVΔGL-Flpo left almost all labeled neurons alive for as long as we imaged them (16 weeks). This confirmed that the Flpo-expressing and Cre-expressing ΔGL viruses are similarly nontoxic to labeled cells, consistent with our expectation that, regardless of the transgene, the drastic reduction in gene expression level caused by deletion of L would eliminate the cytotoxicity caused by the rampant intracellular activity of wild-type and ΔG rabies viruses. These findings suggest that second-generation monosynaptic tracing will be essentially nonperturbative to labeled presynaptic neurons (which are only infected with the ΔGL viruses and not the helper viruses), except to the extent that toxicity to the postsynaptic starting cells might perturb cells presynaptic to them by trophic or other network effects.

We then conducted an experiment to determine how toxic the full second-generation monosynaptic tracing system was to neurons, including the starting cells in which G and L were provided (Fig. 3). Similar to the experiments shown in Fig. 1d-e, we injected the Cre-dependent helper virus combination into visual cortex of PV-Cre x TRE-CB x Ai65F mice, followed by RVGL-Flpo(EnvA) seven days later. For this set of experiments, we additionally implanted a headmount and optical window (see Methods), and we imaged fields of view at or near the injection sites on a two-photon microscope repeatedly over 14 consecutive sessions beginning at two days postinjection and ending at 12 weeks (Fig 3a). Just as for the previous experiments, half of the mice were given doxycycline beginning at two weeks postinjection.

We found that, with or without doxycycline, the majority of tdTomato-labeled cells at the injection sites survived for the full 12 weeks of imaging in most mice. For the mice that did not receive doxycycline, and that therefore had G and L expressing throughout the 12-week experiment, a respectable 63.4% of labeled cells survived through the final imaging session. For the mice that did receive doxycycline, however, the neuronal survival rate was downright impressive: 94.4% of labeled neurons survived (Fig. 3b-h; see also Extended Data Fig. 7; see also Supplementary File 4 for counts of total and surviving cells). Again, there appeared to be no downside to doxycycline administration, as transsynaptic spread to other cortical areas was still widespread in these mice (Fig. 3k).

Although the overall cell survival rate was high, we anticipated that it would be lower for starting neurons, in which G and L are provided and viral replication is therefore restored. In order to determine the survival rate of starting cells, the ideal approach would have been to image both tdTomato (reporting activity of the Flpo expressed by the rabies virus) and mTagBFP2 (coexpressed with G by the second helper virus): neurons that expressed both fluorophores would be both infected by the RVΔGL and expressing G (and by extension L, because both depend on tTA expression) and therefore competent hosts for the RV to replicate within and spread to cells presynaptic to them. However, because the two-photon microscope to which we had access was unfortunately incapable of producing short-wavelength light at sufficient power to allow imaging of mTagBFP2 *in vivo*, we had to rely in indirect measures to estimate the starting cells' survival rates. Note that EGFP, which was coexpressed with TVA, is not a good indication of whether a cell is a starting cell, because, although some of the cells expressing TVA were of course the ones directly infected by the EnvA-enveloped rabies virus, only a subset of such cells also express G (as reported by mTagBFP2: see Supplementary File 2) and are therefore able to support replication and spread of the rabies virus; in any case, at the helper virus concentrations used[46,47], the intrinsic EGFP signal is quite weak and needs to be amplified with immunostaining in order to be clearly discernible.

Following longitudinal two-photon imaging of tdTomato-labeled cells over the full 12 weeks, therefore, we perfused the mice, sectioned the brains in a plane approximately parallel to the imaging plane, then imaged the same regions using confocal microscopy (Fig. 3). This allowed us to image tdTomato as well as mTagBFP2 (for animals that had not received doxycycline), then align the confocal images with the two-photon ones from the 12-week timepoint to identify the surviving double-labeled starting cells (Fig. 3i-j). For those animals that did receive doxycycline, the blue channel of course contained little signal (Fig. 3j); our second goal for the confocal imaging, however, was to confirm that transsynaptic tracing in these mice used for two-photon imaging had been successful (Fig. 3k). For both dox and no-dox conditions, we made the assumption that all cells that had died were starting cells, based on our finding that cells infected solely with the RV∆GL-Flpo without complementation almost invariably survive (Extended Data Fig. 6; see also Chatterjee et al.[2] for extensive characterization of the nontoxicity of ∆GL RV).

In the mice that did not receive doxycycline, in which the surviving starting cells (i.e., those expressing red and blue fluorophores) were visible by confocal microscopy (Fig 3i), we estimated the starting cell survival rate in each mouse as the ratio of the number of cells in the field of view expressing both red and blue fluorophores divided by the sum of that number plus the number of cells that died in that field of view (Fig. 3l & 3n; see Supplementary File 4 for cell counts and calculations). For these no-dox mice, we obtained a survival rate of 53.2% of starting cells.

In the mice that did receive doxycycline, in which surviving starting cells were not identifiable as such by postmortem confocal microscopy because they no longer expressed mTagBFP2 (Fig. 3j), we made the assumption that starting cells made up the same percentage of total tdTomato-labeled neurons in the fields of view in the dox mice as in the no-dox ones, because the experimental conditions were identical apart from the switch to doxycycline two weeks after RV injection. This gave us an estimated number of total starting cells for each mouse; the difference between that and the (very small) number of neurons that had disappeared over the course of the two-photon imaging gave us an estimated number of surviving starting cells. The ratio of the estimated number of surviving starting cells to the estimated total number of starting cells was our estimate of the starting cell survival rate (Fig. 3m & 3n; see Supplementary File 4 for cell counts and calculations). For these dox mice, we obtained an estimated survival rate of 92.3% of starting cells. This is only slightly lower than the 94.4% overall survival rate for labeled neurons in these mice; this makes sense, in our view, given both that the majority of neurons in the field of view were presumably starting cells and that the survival rate should be higher in those mice that received doxycycline to suppress G and L expression than in those that did not.

Longitudinal two-photon calcium imaging of cortical neurons' responses to visual stimuli

Finally, we conducted experiments designed to provide proof of concept for long-term functional imaging of synaptically-connected networks of neurons labeled using second-generation monosynaptic tracing.

We began by making a Flp-dependent jGCaMP7s reporter AAV and conducted pilot studies in PV-Cre mice to determine a dilution that would not itself cause mass cytotoxicity due to overexpression of jGCaMP7s[45,60] (Extended Data Fig. 8). We then conducted an experiment similar in design to the structural imaging study, except that the rabies virus was mixed with the jGCaMP7s AAV before injection and headmount/coverslip implantation (Fig. 4a). We then imaged labeled neurons at or near the injection sites over a series of sessions spanning ten weeks. We imaged the jGCaMP7s signal while the awake mice viewed a series of drifting grating stimuli (Fig. 4b-c); we also imaged tdTomato fluorescence in the same fields of view to confirm that jGCaMP7s expression was restricted to RV-labeled neurons (Fig. 4c). As shown in Fig. 4d-f, as well as Extended Data Figs. 9 and 10, we observed clear orientation tuning curves in many of the labeled neurons. The visual responses of tuned neurons remained stable over the full ten weeks of imaging (Fig 4d-f, and Extended Data Fig. 10). Following the full course of two-photon imaging, we conducted postmortem sectioning and confocal imaging to confirm that the imaged mice had in fact supported intact transsynaptic spread (Extended Data Fig. 11).

Discussion

We have shown here that it is possible to use nontoxic double-deletion-mutant rabies viral vectors to label direct inputs to starting cells targeted based either on their gene expression (Cre lines) or extrinsic projections. We have shown that use of the tet-off system results in little toxicity even to the starting cells, without reducing the efficiency of spread. We have further shown that the apparent low efficiency seen

with the second-generation system in Cre lines may be due simply to the low efficiency of Flpo, as the use of a rabies virus expressing Cre to label inputs to corticostriatal cells was as efficient as the first-generation system. We have further used two-photon functional imaging of live second-generation monosynaptic tracing *in vivo* to show that labeled neurons have normal visual response properties that remain stable over at least ten weeks, the longest we followed them.

It is perhaps surprising that so many starting cells (over 92%) appeared to survive when doxycycline was administered beginning at two weeks postinjection (Fig. 3), even though doxycycline did not reduce the efficiency of transsynaptic spread (Figs. 1 & 2). To an extent, this was not accidental: we designed the system so that we would be able to titrate the level and time course of L expression as necessary to reduce toxicity to starting cells. However, it was undoubtedly fortunate that the very simple protocol of switching mice to high-dose (200 mg/kg) doxycycline chow two weeks after ΔGL rabies virus injection turned out to be sufficient to preserve the great majority of starting cells (at least for cortical cells in the PV-Cre mice that we tested this in). It was even more fortunate that this intervention did not reduce the efficiency of transsynaptic spread in either of the Cre lines or in the corticostriatal experiments but in fact resulted in increased spread in most sets of conditions, although the increases were not statistically significant.

A possible explanation for why administration of doxycycline to suppress G and L expression after an initial two-week period of unrestricted expression could increase transsynaptic spread is that the shutdown of G and L is gradual and incomplete despite the high dose of doxycycline used (200 mg/kg). This is consistent with mTagBFP2 fluorescence still being visible in the dox mice, primarily at the 3-week time point (which is only one week after the mice had been switched to dox chow) but also even at the 5-week time point to a lesser degree; this effect was much more pronounced in the PV-Cre mice than in the DAT-IRES-Cre ones or in the corticostriatal experiments (see Extended Data Figs. 2 and 3 as well as Fig. 2; the detailed counts in Supplementary Files 1, 2, and 3). This presumably means that viral replication continues for quite some time after the switch to doxycycline, at a lower level that is less toxic to cells but that is nevertheless sufficient to label notably (though not significantly, given the low n used for the groups in this study) more presynaptic cells.

An undeniable drawback of the second-generation system introduced here is its slow time course, such as the 2- to 5-week survival times used for the anatomical studies. We presume that this slow time course is due to low L expression from the TRE-CB allele given the low level of tTA expressed by the intentionally-dilute Cre- or Flp-dependent helper virus[46,47]; this hypothesis is consistent with our inability to detect clear mCardinal signal by confocal microscopy (Extended Data Fig. 1) and perhaps also explains the high percentage of surviving starting cells that we found. While a slow time course is inconvenient for busy neuroscientists, it may be the necessary price of preserving the starting cells.

A striking finding from the current study was that, when we switched from an RVΔGL expressing Flpo to a version expressing (mouse-codon-optimized[61]) Cre, the apparent efficiency increased dramatically (Fig. 2). Our working hypothesis is that this is simply due to a difference in inefficiency of the two recombinases, with Cre more faithfully reporting the actual spread of the virus than Flpo. This is consistent with other indications from our experiments that Flpo is less effective than Cre: in the corticostriatal experiments, for example, the Flp-dependent version of the TVA-tTA-expressing helper virus appeared not to work as well as the Cre-dependent one for the first-generation system, necessitating a longer (12d) survival time for that configuration (Fig. 2); the titers of the RVΔGL-Flpo also appeared considerably lower on reporter cells than when we titered on L-expressing cells with nucleoprotein staining (see Methods), whereas the corresponding titers of RVΔGL-Cre were more consistent across the two titering methods.

We note that, even apart from the rabies virus and its complementing gene products, several of the components of the system have the potential to cause cytotoxicity, including tTA[45,62,63], GCaMPs[45,60], and even AAV itself[64]. These can be expected to contribute to the toxicity to starting cells, perhaps making it more remarkable that we found that so many of them survived. The toxicity to starting cells may also depend on the cell type, both because neuron types can be differentially vulnerable to adverse conditions[65,66] and because differential tropism for AAV1[47] (or whatever other serotype might be used for the helper viruses) will change the dosage of tTA, G, L, TVA (and therefore the initial multiplicity of infection by the injected RV), and the fluorophores.

The presynaptic cells, on the other hand, are much less burdened than the postsynaptic ones: because we have found that ΔGL RV by itself (in combination with tdTomato expression in Ai14 or Ai65F mice) does not kill neurons, the vast majority of labeled presynaptic cells can be expected to survive, although residual toxicity to the starting cells postsynaptic to them could cause some remodeling or toxicity via retrograde transneuronal effects[67].

While the second-generation system is somewhat more difficult to implement than the first-generation one in that it requires two additional transgenic alleles (for expressing L and for reporting activity of the recombinase expressed by the RV), in practice this is not burdensome: we have found that the TRE-CB mice can be readily maintained as double homozygotes with the Ai14 or Ai65F alleles, so that production of triply (Figs. 1, 3, & 4) or doubly (Fig. 2) heterozygous mice is easily achieved by a single cross with either a recombinase-expressing (e.g., PV-Cre) or wild-type mouse.

Perhaps importantly, our finding that ΔGL rabies viruses do not spread when not complemented by L expression *in trans*, even when G is provided *in trans*, indicates that deletion of either L or G alone is sufficient to prevents transsynaptic spread. This suggests the possibility of a "third-generation" monosynaptic tracing system, based on single-deletion-mutant ΔL viruses complemented by expression *in trans* of just L. Because of the reduced complexity of complementing with (once again) only a single gene, such a system may have advantages over the second-generation one described here.

References

1. Wickersham, I.R. *et al.* Monosynaptic restriction of transsynaptic tracing from single, genetically targeted neurons. *Neuron* **53**, 639-47 (2007).
2. Chatterjee, S. *et al.* Nontoxic, double-deletion-mutant rabies viral vectors for retrograde targeting of projection neurons. *Nat Neurosci* **21**, 638-646 (2018).
3. Zampieri, N., Jessell, T.M. & Murray, A.J. Mapping sensory circuits by anterograde transsynaptic transfer of recombinant rabies virus. *Neuron* **81**, 766-78 (2014).
4. Yonehara, K. *et al.* Spatially asymmetric reorganization of inhibition establishes a motion-sensitive circuit. *Nature* **469**, 407-10 (2011).
5. Miyamichi, K. *et al.* Cortical representations of olfactory input by trans-synaptic tracing. *Nature* **472**, 191-6 (2011).
6. Schwarz, L.A. *et al.* Viral-genetic tracing of the input-output organization of a central noradrenaline circuit. *Nature* (2015).
7. Wertz, A. *et al.* PRESYNAPTIC NETWORKS. Single-cell-initiated monosynaptic tracing reveals layer-specific cortical network modules. *Science* **349**, 70-4 (2015).
8. Stephenson-Jones, M. *et al.* A basal ganglia circuit for evaluating action outcomes. *Nature* **539**, 289-293 (2016).
9. Beier, K.T. *et al.* Rabies screen reveals GPe control of cocaine-triggered plasticity. *Nature* **549**, 345-350 (2017).
10. Szonyi, A. *et al.* Median raphe controls acquisition of negative experience in the mouse. *Science* **366**(2019).
11. Takahashi, T.M. *et al.* A discrete neuronal circuit induces a hibernation-like state in rodents. *Nature* **583**, 109-114 (2020).
12. Rossi, L.F., Harris, K.D. & Carandini, M. Spatial connectivity matches direction selectivity in visual cortex. *Nature* **588**, 648-652 (2020).
13. Jin, H., Fishman, Z.H., Ye, M., Wang, L. & Zuker, C.S. Top-Down Control of Sweet and Bitter Taste in the Mammalian Brain. *Cell* **184**, 257-271 e16 (2021).
14. Yao, S. *et al.* A whole-brain monosynaptic input connectome to neuron classes in mouse visual cortex. *bioRxiv*, 2021.09.29.459010 (2021).
15. Schmidt, E.R.E. *et al.* A human-specific modifier of cortical connectivity and circuit function. *Nature* (2021).
16. Geiller, T. *et al.* Local circuit amplification of spatial selectivity in the hippocampus. *Nature* (2021).
17. Rancz, E.A. *et al.* Transfection via whole-cell recording in vivo: bridging single-cell physiology, genetics and connectomics. *Nature neuroscience* (2011).
18. Velez-Fort, M. *et al.* A Circuit for Integration of Head- and Visual-Motion Signals in Layer 6 of Mouse Primary Visual Cortex. *Neuron* **98**, 179-191 e6 (2018).
19. Yonehara, K. *et al.* The first stage of cardinal direction selectivity is localized to the dendrites of retinal ganglion cells. *Neuron* **79**, 1078-85 (2013).
20. Rompani, S.B. *et al.* Different Modes of Visual Integration in the Lateral Geniculate Nucleus Revealed by Single-Cell-Initiated Transsynaptic Tracing. *Neuron* **93**, 1519 (2017).
21. Schwarz, M.K. & Remy, S. Rabies virus-mediated connectivity tracing from single neurons. *J Neurosci Methods* **325**, 108365 (2019).
22. Wickersham, I.R., Finke, S., Conzelmann, K.K. & Callaway, E.M. Retrograde neuronal tracing with a deletion-mutant rabies virus. *Nature Methods* **4**, 47-9 (2007).
23. Reardon, T.R. *et al.* Rabies Virus CVS-N2c(DeltaG) Strain Enhances Retrograde Synaptic Transfer and Neuronal Viability. *Neuron* **89**, 711-24 (2016).
24. Albertini, A.A., Ruigrok, R.W. & Blondel, D. Rabies virus transcription and replication. *Advances in virus research* **79**, 1-22 (2011).

25. Prosniak, M., Hooper, D.C., Dietzschold, B. & Koprowski, H. Effect of rabies virus infection on gene expression in mouse brain. *Proc Natl Acad Sci U S A* **98**, 2758-63 (2001).
26. Huang, K.W. & Sabatini, B.L. Single-Cell Analysis of Neuroinflammatory Responses Following Intracranial Injection of G-Deleted Rabies Viruses. *Front Cell Neurosci* **14**, 65 (2020).
27. Komarova, A.V. *et al.* Rabies virus matrix protein interplay with eIF3, new insights into rabies virus pathogenesis. *Nucleic Acids Res* **35**, 1522-32 (2007).
28. Ciabatti, E., Gonzalez-Rueda, A., Mariotti, L., Morgese, F. & Tripodi, M. Life-Long Genetic and Functional Access to Neural Circuits Using Self-Inactivating Rabies Virus. *Cell* **170**, 382-392 e14 (2017).
29. Matsuyama, M. *et al.* "Self-inactivating" rabies viruses are just first-generation, ΔG rabies viruses. *bioRxiv*, 550640 (2019).
30. Jin, L. *et al.* Rabies virus with a destabilization domain added to its nucleoprotein spreads between neurons only if the domain is removed. *bioRxiv*, 550640 (2021).
31. Young, J.A., Bates, P. & Varmus, H.E. Isolation of a chicken gene that confers susceptibility to infection by subgroup A avian leukosis and sarcoma viruses. *J Virol* **67**, 1811-6 (1993).
32. Bates, P., Young, J.A. & Varmus, H.E. A receptor for subgroup A Rous sarcoma virus is related to the low density lipoprotein receptor. *Cell* **74**, 1043-51 (1993).
33. Wall, N.R., Wickersham, I.R., Cetin, A., De La Parra, M. & Callaway, E.M. Monosynaptic circuit tracing in vivo through Cre-dependent targeting and complementation of modified rabies virus. *Proceedings of the National Academy of Sciences of the United States of America* (2010).
34. Watabe-Uchida, M., Zhu, L., Ogawa, S.K., Vamanrao, A. & Uchida, N. Whole-brain mapping of direct inputs to midbrain dopamine neurons. *Neuron* **74**, 858-73 (2012).
35. Kohara, K. *et al.* Cell type-specific genetic and optogenetic tools reveal hippocampal CA2 circuits. *Nat Neurosci* **17**, 269-79 (2014).
36. Liu, K. *et al.* Lhx6-positive GABA-releasing neurons of the zona incerta promote sleep. *Nature* **548**, 582-587 (2017).
37. Lai, Y., Yue, Y. & Duan, D. Evidence for the failure of adeno-associated virus serotype 5 to package a viral genome > or = 8.2 kb. *Mol Ther* **18**, 75-9 (2010).
38. Wu, Z., Yang, H. & Colosi, P. Effect of genome size on AAV vector packaging. *Molecular therapy : the journal of the American Society of Gene Therapy* **18**, 80-6 (2010).
39. Dong, B., Nakai, H. & Xiao, W. Characterization of genome integrity for oversized recombinant AAV vector. *Molecular therapy : the journal of the American Society of Gene Therapy* **18**, 87-92 (2010).
40. Hirsch, M.L., Wolf, S.J. & Samulski, R.J. Delivering Transgenic DNA Exceeding the Carrying Capacity of AAV Vectors. *Methods Mol Biol* **1382**, 21-39 (2016).
41. Gossen, M. & Bujard, H. Tight control of gene expression in mammalian cells by tetracycline-responsive promoters. *Proc Natl Acad Sci U S A* **89**, 5547-51 (1992).
42. Chu, J. *et al.* Non-invasive intravital imaging of cellular differentiation with a bright red-excitable fluorescent protein. *Nat Methods* **11**, 572-8 (2014).
43. Zeng, H. *et al.* An inducible and reversible mouse genetic rescue system. *PLoS genetics* **4**, e1000069 (2008).
44. Madisen, L. *et al.* Transgenic mice for intersectional targeting of neural sensors and effectors with high specificity and performance. *Neuron* **85**, 942-58 (2015).
45. Daigle, T.L. *et al.* A Suite of Transgenic Driver and Reporter Mouse Lines with Enhanced Brain-Cell-Type Targeting and Functionality. *Cell* **174**, 465-480 e22 (2018).
46. Lavin, T.K., Jin, L. & Wickersham, I.R. Monosynaptic tracing: a step-by-step protocol. *J Chem Neuroanat*, 101661 (2019).
47. Lavin, T.K., Jin, L., Lea, N.E. & Wickersham, I.R. Monosynaptic Tracing Success Depends Critically on Helper Virus Concentrations. *Front Synaptic Neurosci* **12**, 6 (2020).
48. Sternberg, N. & Hamilton, D. Bacteriophage P1 site-specific recombination. I. Recombination between loxP sites. *J Mol Biol* **150**, 467-86 (1981).
49. Atasoy, D., Aponte, Y., Su, H.H. & Sternson, S.M. A FLEX switch targets Channelrhodopsin-2 to multiple cell types for imaging and long-range circuit mapping. *The Journal of neuroscience : the official journal of the Society for Neuroscience* **28**, 7025-30 (2008).
50. Cormack, B.P., Valdivia, R.H. & Falkow, S. FACS-optimized mutants of the green fluorescent protein (GFP). *Gene* **173**, 33-8 (1996).
51. Thastrup, O., Tullin, S., Poulsen, L.K. & Bjorn, S.P. Fluorescent proteins. (2001).
52. Subach, O.M., Cranfill, P.J., Davidson, M.W. & Verkhusha, V.V. An enhanced monomeric blue fluorescent protein with the high chemical stability of the chromophore. *PloS one* **6**, e28674 (2011).
53. Sadowski, P.D. The Flp recombinase of the 2-microns plasmid of Saccharomyces cerevisiae. *Prog Nucleic Acid Res Mol Biol* **51**, 53-91 (1995).
54. Raymond, C.S. & Soriano, P. High-efficiency FLP and PhiC31 site-specific recombination in mammalian cells. *PloS one* **2**, e162 (2007).
55. Backman, C.M. *et al.* Characterization of a mouse strain expressing Cre recombinase from the 3' untranslated region of the dopamine transporter locus. *Genesis* **44**, 383-90 (2006).

56. Hippenmeyer, S. *et al.* A developmental switch in the response of DRG neurons to ETS transcription factor signaling. *PLoS Biol* **3**, e159 (2005).
57. Kranz, A. *et al.* An improved Flp deleter mouse in C57Bl/6 based on Flpo recombinase. *Genesis* **48**, 512-20 (2010).
58. Tervo, D.G. *et al.* A Designer AAV Variant Permits Efficient Retrograde Access to Projection Neurons. *Neuron* **92**, 372-382 (2016).
59. Madisen, L. *et al.* A robust and high-throughput Cre reporting and characterization system for the whole mouse brain. *Nature neuroscience* **13**, 133-40 (2010).
60. Steinmetz, N.A. *et al.* Aberrant Cortical Activity in Multiple GCaMP6-Expressing Transgenic Mouse Lines. *eNeuro* **4**(2017).
61. Koresawa, Y. *et al.* Synthesis of a new Cre recombinase gene based on optimal codon usage for mammalian systems. *Journal of biochemistry* **127**, 367-72 (2000).
62. Han, H.J. *et al.* Strain background influences neurotoxicity and behavioral abnormalities in mice expressing the tetracycline transactivator. *J Neurosci* **32**, 10574-86 (2012).
63. Hoyng, S.A. *et al.* Developing a potentially immunologically inert tetracycline-regulatable viral vector for gene therapy in the peripheral nerve. *Gene Ther* **21**, 549-57 (2014).
64. Xiong, W. *et al.* AAV cis-regulatory sequences are correlated with ocular toxicity. *Proc Natl Acad Sci U S A* **116**, 5785-5794 (2019).
65. Hedreen, J.C. & Folstein, S.E. Early loss of neostriatal striosome neurons in Huntington's disease. *J Neuropathol Exp Neurol* **54**, 105-20 (1995).
66. Burke, R.E. & Baimbridge, K.G. Relative loss of the striatal striosome compartment, defined by calbindin-D28k immunostaining, following developmental hypoxic-ischemic injury. *Neuroscience* **56**, 305-15 (1993).
67. Fricker, M., Tolkovsky, A.M., Borutaite, V., Coleman, M. & Brown, G.C. Neuronal Cell Death. *Physiol Rev* **98**, 813-880 (2018).

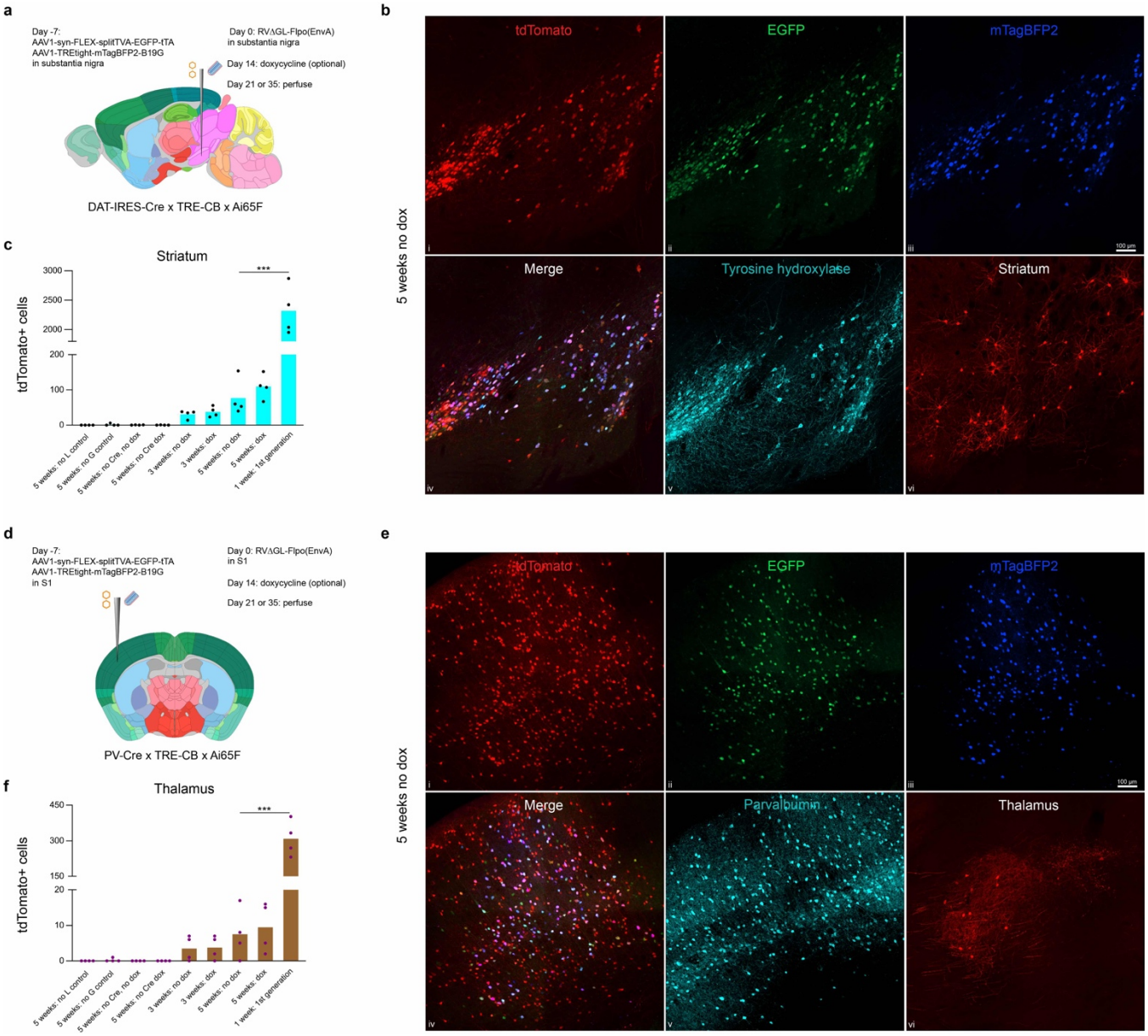

Fig. 1: Second-generation (ΔGL) rabies viral vectors spread between neurons when complemented with both glycoprotein and polymerase expression *in trans.* **a,** Experimental design for labeling inputs to dopaminergic cells in the substantia nigra, pars compacta (SNc). The same helper virus combination used for the first-generation system was injected into the substantia nigra of triple transgenic mice: DAT-IRES-Cre (to select the starting cells) x "TRE-CB" (providing RV polymerase *in trans*) x Ai65F (Flp-dependent tdTomato reporter)). An EnvA-enveloped ΔGL rabies virus expressing Flpo was injected seven days later. For the "dox" conditions, mice were switched to doxycycline-containing food 14 days after rabies virus injection, to suppress expression of the viral polymerase and glycoprotein after viral spread. **b,** Example of labeled cells five weeks after rabies virus injection, without doxycycline. **b.i-v,** Injection site in SNc, with many cells co-expressing tyrosine hydroxylase (indicating the dopaminergic cells), EGFP (expressed by the first helper virus), mTagBFP2 (expressed by the second helper virus), and tdTomato (reporting activity of the Flpo-expressing rabies virus). Scale bar in **iii**: 100 µm, applies to all images. **b.vi,** Medium spiny neurons in striatum labeled by the ΔGL rabies virus. **c,** Counts of labeled striatal cells in all conditions tested. Omitting any of L, G, or Cre resulted in almost no labeled cells in striatum. Administration of doxycycline to suppress G and L expression after the first two weeks, as well as longer survival time (5 weeks vs 3 weeks), both resulted in increased transsynaptic spread, although most comparisons were not statistically significant (see Supplementary File 1 for all counts and statistical comparisons). The first-generation system (with a much shorter survival time) labeled many more cells than all conditions tested for this implementation of the second-generation one. **d,** Experimental design for labeling inputs to parvalbumin-expressing cells

in primary somatosensory cortex (S1). **e,** Example of labeled cells five weeks after rabies virus injection, without doxycycline. **e.i-v,** Injection site in S1, with many cells coexpressing parvalbumin, reporters of both helper viruses, and tdTomato reporting activity of the rabies virus. In addition to these starting cells, many putatively presynaptic cells expressing tdTomato are present. Scale bar in iii: 100 µm, applies to all images. **e.vi,** Relay neurons in ipsilateral thalamus labeled by the ∆GL rabies virus. **f,** Counts of labeled thalamic cells in all conditions tested. Again, omitting any of L, G, or Cre resulted in little or no transsynaptic spread, provision of doxycyline increased transsynaptic spread somewhat, and longer survival time resulted in more spread. The first-generation system again labeled many more cells than did this implementation of the second-generation system (see Supplementary File 2 for all statistical comparisons and p-values).

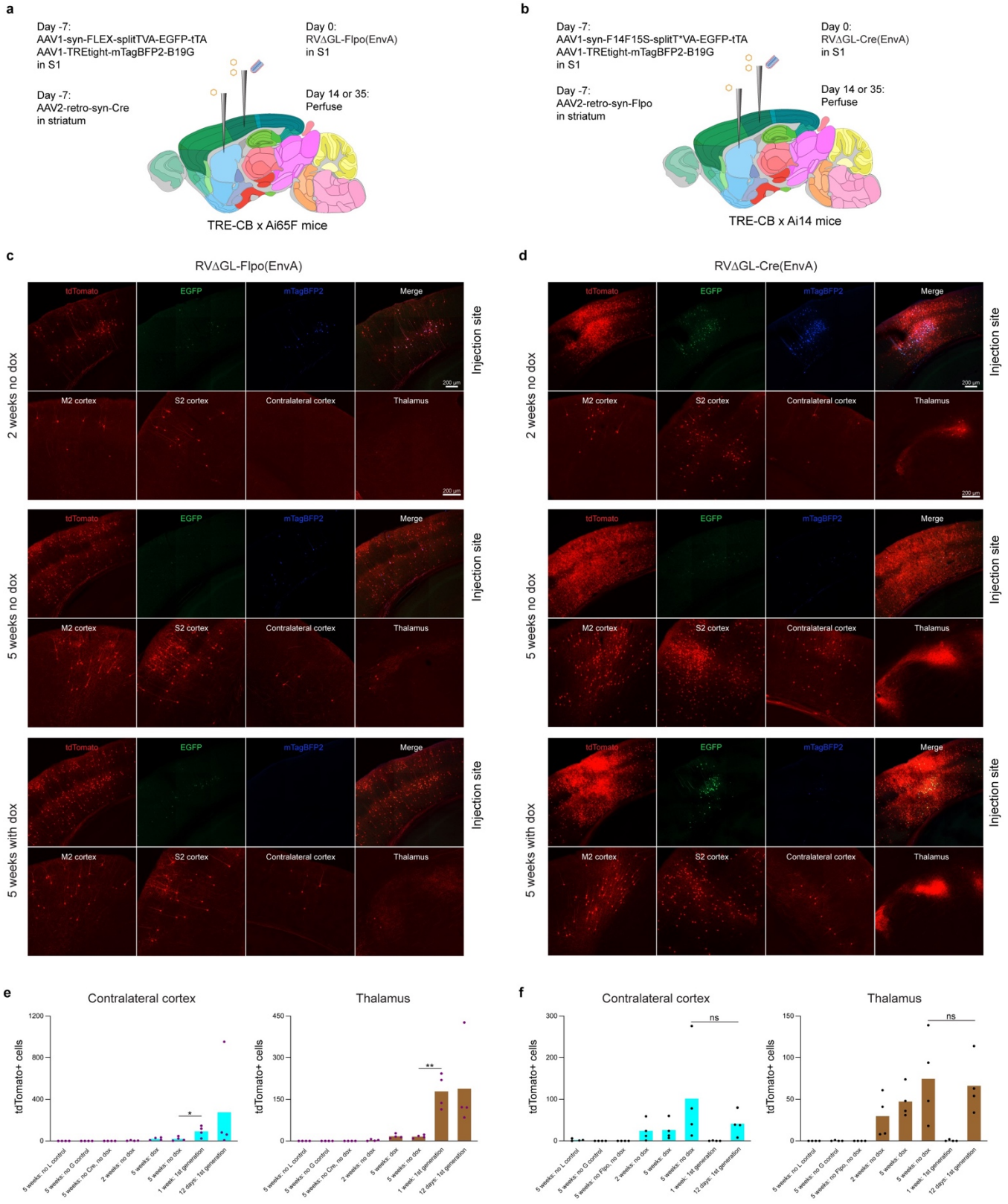

Fig. 2: Second-generation monosynaptic tracing of inputs to corticostriatal neurons: using ΔGL virus expressing Cre, rather than Flpo, results in efficiency comparable to that of the first-generation system. a-b, Experimental design. Corticostriatal neurons were retrogradely targeted by an rAAV2-retro expressing either Cre or Flpo injected into dorsolateral striatum, with a Cre- or Flp-dependent helper virus combination injected into S1; the EnvA-enveloped ΔGL rabies virus expressing either Flpo or Cre was injected in S1 seven days later. **c,** Images of cells labeled with the Flpo-expressing RV. Labeled cells are found in ipsilateral secondary motor and somatosensory cortices, in contralateral S1, and ipsilateral thalamus. Scale bars: 200 µm, apply to all images. **d,** With the Cre-expressing RV, labeled cells are found in the same regions but in much greater numbers. **e-f,** Counts of

labeled cells in contralateral S1 and ipsilateral thalamus for RV∆GL-Flpo (**e**) and RV∆GL-Cre (**f**). As found in the previous experiments (Fig. 1), spread of both RVs is greater at five weeks than three weeks, and omission of L, G, or Cre/Flpo results in trivial numbers of labeled neurons. Also as found in the previous experiments, the Flpo-expressing ∆GL RV labeled far fewer cells than did a first-generation version. However, the Cre-expressing ∆GL RV labeled many more cells than the Flpo-expressing version in all experimental conditions, in fact exceeding the numbers labeled by the matched first-generation versions, although those differences were not significant (see Supplementary File 3 for counts and statistical comparisons).

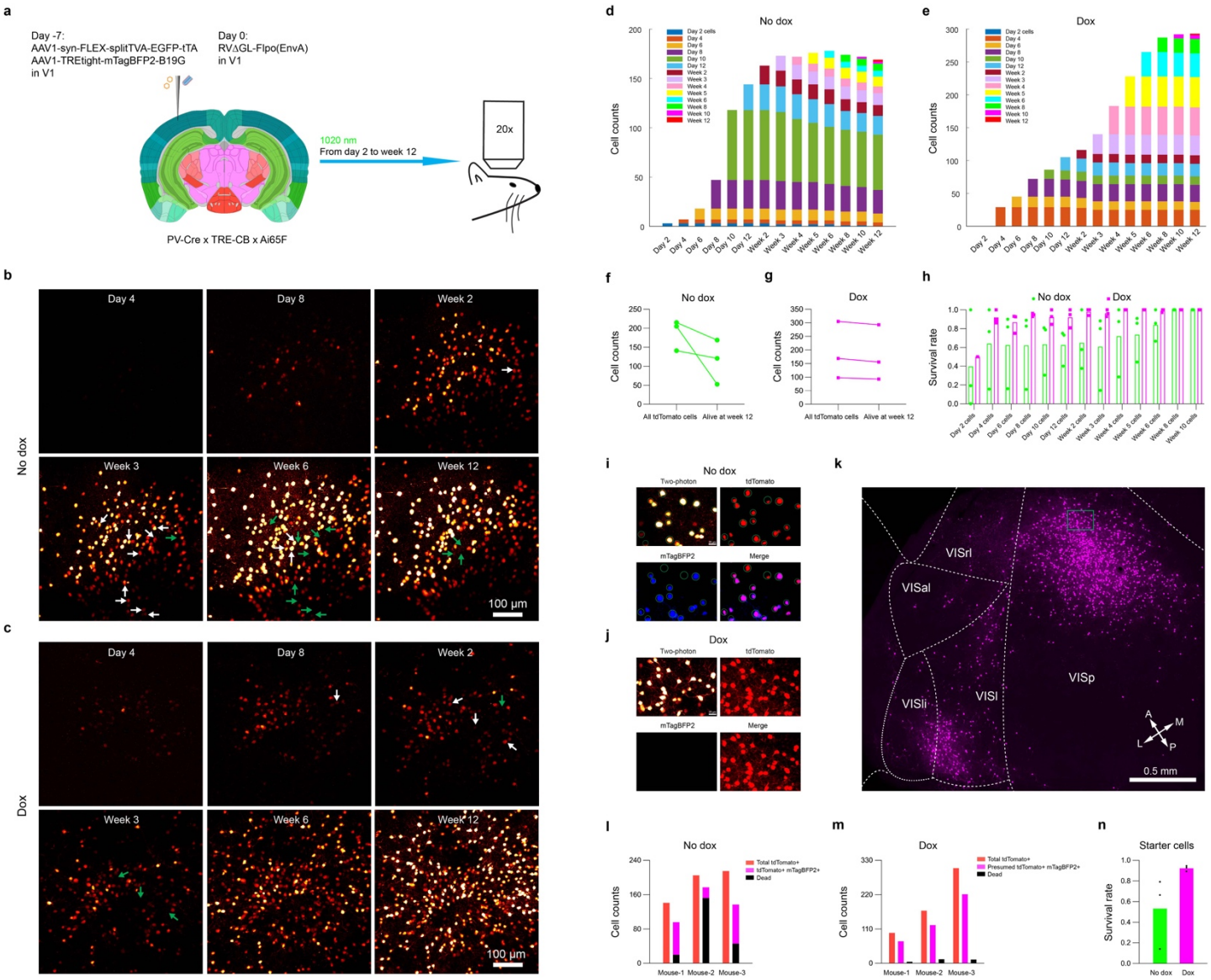

Fig. 3: Longitudinal structural two-photon imaging *in vivo*: second-generation monosynaptic tracing preserves >90% of starting postsynaptic cells. a, Schematic of virus injection and longitudinal two-photon imaging. After injection of the two helper AAVs followed by RVΔGL-Flpo(EnvA) in PV-Cre x TRE-CB x Ai65F as described in Fig. 1, the injection site was imaged on a two-photon microscope repeatedly for 12 weeks after RV injection. **b-c,** Representative two-photon images at different timepoints of tdTomato-labelled neurons in the injection site in V1. The 'No dox' group (b) was fed with regular food throughout, whereas the 'Dox' group (c) was fed with doxycycline food (200 mg/kg) starting at two weeks after RV injection until perfusion at week 12, in order to suppress rabies viral polymerase and glycoprotein expression. Arrows indicate example cells that are alive up to one timepoint (white arrows) but that are missing subsequently (green arrows). In this example, a total of 46 out of 215 cells were lost in the 'No dox' group, whereas 12 out of 305 cells were lost in the 'Dox' group. Scale bar = 100 µm. **d,** Cell counts from all 14 timepoints in one of the 'No dox' mice. This is the same mouse as shown in **b**. Bar height for each color indicates the number of cells that were first visible at the corresponding timepoint that are still visible at the timepoint shown on the X axis; for example, the dark green bars indicate the number of cells that were first visible on day 10 that are identifiable at each timepoint from 10 days onward. **e,** Cell counts from all 14 timepoints in one of the 'Dox' mice. This is the same mouse as shown in **c**. **f,** Total number of imaged cells and number of cells present at the last imaging timepoint for each of the 'No dox' mice. **g,** Total number of imaged cells and number of cells present at the last imaging timepoint for each of the 'Dox' mice. Administration of doxycycline greatly reduces cell attrition. **h,** Survival rates of cells that appeared at each time point for each mouse in both 'Dox' and 'No dox' groups. Each data point represents the fraction of cells that first became visible at that timepoint that were still present at the last (12-week) timepoint. **i,** Aligned 12-week two-photon

image (top left) and postmortem confocal images (tdTomato, mTagBFP2, and merged) of an FOV from a ‘No dox’ mouse (the same mouse as used for panel **b**). Cells found by confocal imaging to have expressed both tdTomato (reporting rabies virus activity) and mTagBFP2 (reporting G expression) were considered to be "starting cells", along with the cells that died during the 12 weeks of two-photon imaging. Scale bar: 20 μm. **j,** Aligned 12-week two-photon image (left) and postmortem confocal image of an FOV from a ‘Dox’ mouse (the same mouse as used for panel **c**). Because doxycycline shut off mTagBFP2 expression along with expression of G and L, it was not possible for us to directly determine the surviving number of starting cells in ‘Dox‘ mice; for this group, we used an indirect estimate, as shown in panel **m** below. Scale bar: 20 μm. **k,** Large-scale confocal image of labeled neurons in multiple visual cortical areas in the same ‘Dox’ mouse. The green rectangle indicates the FOV shown in **j**. This demonstrates that the transsynaptic spread of ΔGL virus was intact in the mice used for these imaging experiments, just as in the mice used for the similar experiments shown in previous figures. **l,** Counts for each of the ‘No dox’ mice of the total number of imaged tdTomato+ cells (red), the number of cells that disappeared (black), and the number of cells found by postmortem confocal imaging to have expressed both tdTomato and mTagBFP2 and which therefore were considered surviving starting cells (magenta). The fraction of surviving starting cells for each of these ‘No dox’ mice was calculated as the ratio (magenta)/(black + magenta). **m,** Counts for each of the ‘Dox‘ mice of the total number of imaged tdTomato+ cells (red), the number of cells that disappeared (black), and the *assumed number of total starting cells* (magenta) based on the assumption that the same fraction of total tdTomato+ cells were starting cells in the ‘Dox‘ mice as in the otherwise-identical ‘No dox‘ mice. The fraction of surviving starting cells for each of these ‘Dox’ mice was estimated as the ratio (magenta - black)/(magenta). All counts and calculations used for estimating starting cell survival rates are given in Supplementary File 4. **n,** Calculated rates of starting cell survival for ‘Dox‘ and ‘No dox‘ groups. Administration of doxycycline at two weeks postinjection to suppress expression of the two deleted viral genes markedly increases cell survival rate from 53.2% (‘No dox‘) to 92.3% (‘Dox’).

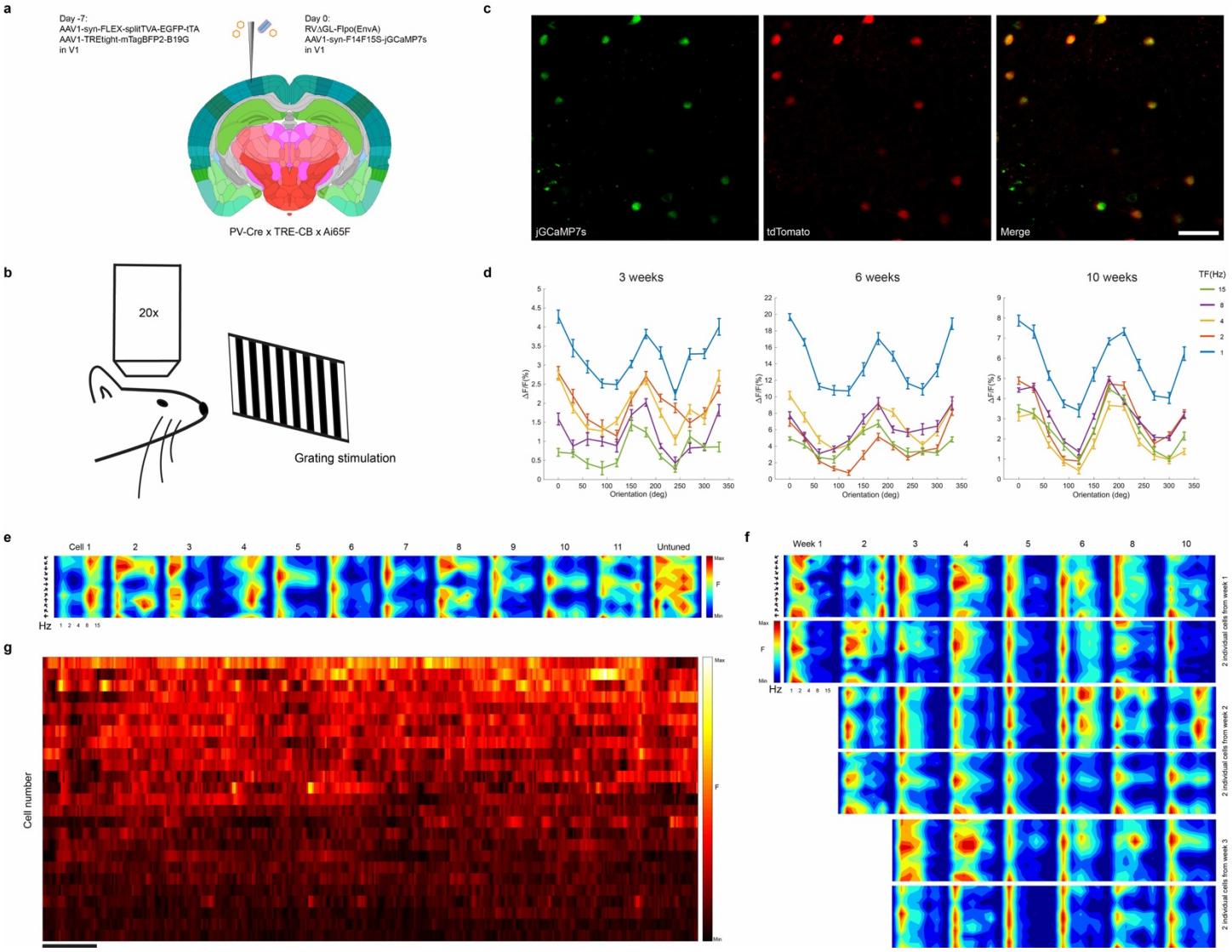

Fig. 4: Longitudinal functional two-photon imaging: labeled neurons' visual response properties remain stable over at least ten weeks. a, The experimental design was similar to that shown in Fig. 3 but with a Flp-dependent jGCaMP7s AAV injected along with the rabies virus. **b,** Following the virus injections, the injection site was imaged on a two-photon microscope while the awake mice were presented with drifting grating stimuli of different orientations and temporal frequencies, repeatedly for 10 weeks after RV injection. **c,** Representative two-photon field of view of neurons expressing jGCaMP7s (green channel) and tdTomato (red channel). Scale bar: 50 µm. **d,** Tuning curves of a jGCaMP7s-expressing neuron obtained with drifting gratings presented at 12 directions of motion and 5 temporal frequencies (TF), repeated 10 times (mean Δ F/F ± s.e.m.) at three different time points (left: week 3; middle: week 6; right: week 10). **e,** Tuning patterns at week 10 of 11 jGCaMP7s-expressing neurons showing clear preferred direction tuning, as wells as the tuning pattern of an untuned neuron, representative of roughly half of imaged cells. **f,** Direction tuning patterns of six individual cells recorded at multiple time points (from week 1 to week 10). Top two cells became visible at week one; the middle two appeared at week two, and the bottom two cells appeared at week three. Tuning patterns remain stable over the entire imaging period. **g,** Single-cell fluorescence time courses for 25 cells, showing activity over the first 120 s of visual stimulation. Cells are ranked in descending order of total activity. Scale bar: 10 s.

Methods

All experiments involving animals were conducted according to NIH guidelines and approved by the MIT Committee for Animal Care. Mice were housed 1-5 per cage under a normal light/dark cycle for all experiments.

Cloning

pAAV-syn-F14F15S-jGCaMP7s (Addgene 178514) was made by cloning a Flp-dependent FLEX arrangement of mutually-incompatible FRT sites[68] into pAAV-synP-FLEX-EGFP-B19G (Addgene 59333) followed by the jGCaMP7s[69] gene from pGP-CMV-jGCaMP7s (Addgene 104463).

pAAV-syn-FLEX-tTA (Addgene 178516) was made by cloning a codon-optimized tet transactivator gene[70] into pAAV-synP-FLEX-EGFP-B19G (Addgene 59333).

pAAV-syn-Flpo (Addgene 174378) and pAAV-syn-mCre (Addgene 178515) were made by replacing the FLEX cassette from pAAV-synP-FLEX-EGFP-B19G (Addgene 59333) with mouse-codon-optimized genes for Flp[54] and Cre[61].

pCAG-hypBase was made by synthesizing a fragment encoding the "hyperactive" piggyBac transposase iPB7[71] and cloning into the EcoRI & NotI sites of pCAG-GFP [72] (Addgene 11150).

The piggyBac plasmid pB-CAG-B19L-IRES-mCherry-WPRE-BGHpA (Addgene 178518) was made by cloning the CAG promoter from pCAG-B19G (Addgene 59921), the SAD B19 L gene, the EMCV IRES[73], the mCherry[74] gene, and the woodchuck post-transcriptional regulatory element and bovine growth hormone polyadenylation signal from pCSC-SP-PW-GFP (Addgene 12337), into PB-CMV-MCS-EF1-Puro (System Biosciences #PB510B-1).

The "TLoop"-style[75] lentiviral transfer vectors pLV-TTBG (Addgene 115232) and pLV-TTBL (Addgene 115233) were made by replacing the CMV promoter and EGFP gene in pCSC-SP-PW-GFP (Addgene 12337) with the leaky tetracycline response element from pAAV-FLEX-hGTB (Addgene 26196) followed by a tricistronic open reading frame consisting of the genes for the "improved tetracycline transactivator" itTA[76], mTagBFP2[52], and either the glycoprotein or polymerase gene, respectively, of the rabies virus SAD B19 strain, separated by P2A elements.

Mouse strains

Mice used in this study were crosses (triple transgenic for DAT-IRES-Cre and PV-Cre experiments, double transgenic for corticostriatal experiments, double or single transgenic (either Cre-negative or L-negative) for control experiments) of the following strains, all in a C57BL/6J (Jackson Laboratory 000664) background:

PV-Cre[56], DAT-IRES-Cre[55], and Ai14[59] were purchased from Jackson Laboratory (catalog #s 017320, 006660, and 007914).

The Flp-dependent tdTomato reporter line Ai65F was obtained in our case by crossing the Cre- and Flp-dependent tdTomato double-reporter line Ai65D[44] (Jackson Laboratory 021875) to the Cre deleter line Meox2-Cre[77] (Jackson Laboratory 003755), then breeding out the Meox2-Cre allele. An equivalent Ai65F line, made using a different Cre deleter line, was described in Daigle et al. '18[45] and is now available from Jackson Laboratory with catalog # 032864).

The L-expressing mouse line TRE-CB (TRE-tight-mCardinal-P2A-B19L, being distributed by Jackson Laboratory with catalog # 036974) was generated by cloning the genes for mCardinal[42] and the rabies virus (SAD B19) polymerase, separated by a picornavirus 2A element[78], into "Ai62(TITL-tdT) Flp-in replacement vector" (Addgene 61576), to make the Flp-in construct "TRE-mCardinal-P2A-B19L Flp-in vector" (Addgene # 178519). The lox-stop-lox sequence present in the original Flp-in vector was removed to make the new construct, so that the tetracycline response element TRE-tight[79] drives mCardinal-P2A-B19L directly with no dependence on Cre recombination. This plasmid was then used for FLP-mediated targeted insertion into the TIGRE locus[43] in Ai99 embryonic stem cells as described[45]. Clones verified as containing the correct insert were used for production of knock-in mice by the Mouse ES Cell & Transgenic Facility at the Koch Institute for Integrative Cancer Research at MIT. All subsequent breeding steps were with mice of a C57BL/6J background.

Production of lentiviral vectors for making cell lines

Lentiviral vectors were made as described[80] but with the VSVG expression vector pMD2.G (Addgene 12259) as the envelope plasmid and with the following transfer vectors:

pLV-TTBL (described above), to make the L-expressing lentiviral vector LV-TTBL(VSVG),

pLV-U-TVA950 (Addgene 115236), to make the TVA-expressing lentiviral vector LV-U-TVA950(VSVG)

Production of cell lines

To make the L-expressing cell line BHK-B19L, BHK-21 cells (ATCC# CCL-10) were transfected with pCAG-hypBase and pB-CAG-B19L-IRES-mCherry-WPRE-BGHpA; the cells were expanded into two 15c plates, then resuspended and sorted on a BD FACS Aria to collect the brightest 5% of mCherry-expressing cells.

BHK-B19L-TVA950 cells were made by infecting BHK-B19L cells (described above) with LV-U-TVA950(VSVG) at a multiplicity of infection of approximately 100. Cells were then expanded and frozen in medium containing 10% DMSO for subsequent use.

The BHK-EnvA2-TTBL2 cell line, expressing both the "EnvARGCD" fusion protein[1] and the RV polymerase, was made by infecting BHK-EnvA2 cells[81] with the L-expressing lentiviral vector LV-TTBL(VSVG) (described above) at a multiplicity of infection of approximately 100. The cells were expanded into three 15 cm plates, then sorted on a BD FACS Aria to collect those cells with the highest 2% of both green (EnvA) and blue (L) fluorescence. After expanding the collected cells again, we observed that blue fluorescence was so dim as to be difficult to detect by eye; we therefore sorted the cells a second time, again retaining cells with the brightest 2% fluorescence in both channels. The twice-sorted cells, now called BHK-EnvA2-TTBL2, were expanded again and frozen in medium containing 10% DMSO for subsequent use.

Production and titering of adeno-associated viruses

AAV genome plasmids pAAV-syn-FLEX-splitTVA-EGFP-tTA (Addgene 100798) and pAAV-TREtight-mTagBFP2-B19G (Addgene 100799) have been described previously[36]. These genomes were packaged in serotype 1 AAV capsids by Addgene (catalog numbers 52473-AAV1, 100798-AAV1, and 100799-AAV1). The two helper AAVs from Addgene were diluted in Dulbecco's phosphate-buffered saline (DPBS) (Thermo, 14190-250) to final titers of 7.22e10 gc/mL for AAV1-syn-FLEX-splitTVA-EGFP-tTA and 6.50e11 gc/mL for AAV-TREtight-mTagBFP2-B19G, then combined in a 50/50 ratio by volume before injection. AAVs from Addgene were initially thawed and aliquoted in 20x 5ul aliquots; to make working dilutions, a 5ul aliquot of undiluted virus was thawed, diluted in DPBS (Thermo Fisher 14190-250) to the desired working dilutions (1:20 or 1:200)[46,47]. pAAV-syn-FLEX-tTA (described above) was packaged as serotype 1 by the UNC Vector Core with titer of 2.51E+12 gc/mL.

rAAV2-retro-syn-Cre, rAAV2-retro-syn-Flpo, and AAV1-syn-F14F15S-jGCaMP7s were made by transfecting 8x15c plates (per virus) of HEK 293T cells using Xfect transfection reagent (Takara 631318). Briefly, plates were treated with poly-L-lysine solution were transfected with pAAV vector, pHelper (Cellbiolabs VPK-421), and the appropriate rep/cap plasmid ("rAAV2-retro helper" (Addgene 81070) or pAAV-RC1 (Cellbiolabs VPK-421)). 4 hours after transfection, the medium from plates was aspirated and replaced with 15mL DMEM (Thermo #11995-081) containing 2% fetal bovine serum (FBS) (HyClone SH30071.02) and antibiotic/antimycotic (Thermo Fisher 15240-062). 72 hours after transfection, the supernatants were collected from each plate and replaced again with 15mL DMEM with 2% FBS and antibiotic/antimycotic. Supernatants were stored in 50mL tubes at 4°C. 120 hours after transfection, cells and supernatants were collected and transferred into sterile 50mL tubes. Cells were pelleted by centrifugation and washed with DPBS, and supernatants were transferred into a sterile bottle for PEG precipitation. Cells were lysed by four freeze/thaw cycles and stored at -80°C until final thaw and purification steps. 50mL of cold 40% polyethylene glycol 8000 (PEG) in 2.5M NaCl was added to 250mL clarified supernatants and mixed thoroughly. This solution was incubated at 4°C overnight, then transferred into sterile 50mL tubes and centrifugated at 4000 RCF for 30 minutes @ 4°C. Supernatants were discarded and pellets resuspended in a total of 1mL 150mM NaCl, 50mM Tris buffer. For final purification steps, cell pellets were combined with PEG-precipitated virus, treated with Benzonase nuclease (250U/uL) for 30 minutes at 37°C, then centrifugated at 7188 RCF for 30 minutes at 4°C. The clarified lysate was transferred to Optiseal tubes (Beckman #361625) containing layered gradients of iodixanol (15%, 25%, 40%, and 54% iodixanol solutions). Tubes were ultracentrifugated in a Beckman 70 Ti fixed-angle rotor at 70,000 rpm for 1hr 40min at 15°C on a WX 80+ centrifuge (Thermo Scientific). The layers containing virus were carefully removed from between the 40% and 54% iodixanol layers, filtered through 0.22um polyethersulfone (PES) membrane syringe filters, and concentrated in Amicon Ultra-15 Centrifuge Units (Millipore #UFC910008), with three full buffer exchanges with DPBS to remove all residual iodixanol. Each batch of virus was concentrated to a final

volume of 250-300 µL total, aliquoted in 5 µl aliquots and stored at -80°C, and titered by quantitative PCR.

Production of rabies viruses

EnvA-enveloped ΔG rabies viruses were made as described previously[29,30,81,82], using genome plasmids pRVΔG-4Flpo (Addgene 122050) and pRVΔG-4Cre (Addgene 98034).

EnvA-enveloped ΔGL rabies viruses were rescued in 15 cm plates as described[2] using genome plasmids pRVΔGL-4Flpo (Addgene 98040) and pRVΔGL-4Cre (Addgene 98039). Supernatants from rescue plates were passaged on 15 cm plates of HEK 293T/17 cells (ATCC) transfected with pLV-TTBG and pLV-TTBL (described above) using Xfect transfection reagent (Takara 631318) according to the manufacturer's protocol. Supernatants were titered on reporter cells[2] and used to infect BHK-EnvA2-TTBL2 cells (described above) at a multiplicity of infection of approximately two. Supernatants from these producer cells were collected and purified as described[81,82].

Titering of rabies viruses

Recombinase-expressing rabies viruses were titered primarily on the reporter cell lines 293T-FLEX-BC, 293T-F14F15S-BC, 293T-FLEX-BC-TVA and 293T-F14F15S-BC-TVA as described[29,30]. For the corticostriatal experiment, in order to directly compare viral titers in a way that did not depend on the efficacy of the encoded recombinases, we made the BHK-B19L-TVA950 cell line (described above), which expresses both TVA, to allow infection by EnvA-enveloped viruses, and L, in order to allow intracellular replication of ΔGL viruses so that infected cells could be clearly labeled using immunostaining against the rabies virus nucleoprotein. For head-to-head comparison of titers of RVΔGL-Cre(EnvA), RVΔGL-Flpo(EnvA), RVΔG-Cre(EnvA), and RVΔG-Flpo(EnvA): 293T-TVA800[83] and BHK-B19L-TVA950 cells (see above) were infected with serial dilutions of first- and second-generation vectors, respectively. Three days after infection, cells were fixed with 4% paraformaldehyde in PBS and immunostained with a FITC-conjugated anti-nucleocapsid monoclonal antibody blend (Light Diagnostics Rabies DFA, EMD Millipore, catalog # 5100) diluted 1:100 in 1% BSA, 0.1% Triton in PBS. Immunolabeled cells were analyzed by flow cytometry to determine titers as described[81].

Stereotaxic injections

300 nl of helper AAV mixture (AAV1-syn-FLEX-splitTVA-EGFP-tTA (diluted to 7.22E+10 GC/mL) mixed with AAV1-TREtight-mTagBFP2-B19G (diluted to 6.50E+11) in a 50/50 ratio by volume) was injected into either primary somatosensory cortex or substantia nigra pars compacta (see below for stereotaxic coordinates) of anesthetized adult mice using a stereotaxic instrument (Stoelting Co., 51925) and a custom injection apparatus consisting of a hydraulic manipulator (Narishige, MO-10) with headstage coupled via custom adaptors to a wire plunger advanced through pulled glass capillaries (Drummond, Wiretrol II) back-filled with mineral oil and front-filled with viral vector solution. We have described this injection system in detail previously[46]. Injection coordinates for substantia nigra pars compacta were: anteroposterior (AP) = -3.00 mm with respect to (w.r.t.) bregma, lateromedial (LM) = +1.50 mm w.r.t bregma, dorsoventral (DV) = -4.20 mm w.r.t the brain surface); injection coordinates for somatosensory cortex were: AP = -0.58 mm w.r.t. bregma, LM = 3.00 mm w.r.t. bregma, DV = -1.00 mm w.r.t the brain surface. Seven days after AAV injection, 500 nl (PV-Cre and DAT-IRES-Cre) of RVΔGL-Flpo(EnvA) (7.67E+08 iu/mL) was injected at the same injection site as the AAVs. Adult mice of both sexes were used.

For the corticostriatal experiments, 200 nl of AAV2-retro-syn-Flpo (1.16E+13 GC/mL; Ai14 or Ai14 x TRE-CB mice) or AAV2-retro-synP-mCre (1.48E+13 GC/mL, diluted to 1.16E+13 GC/mL for matching to the Flpo version; Ai65F or Ai65F x TRE-CB mice) was injected into dorsolateral striatum (AP = +0.74 mm w.r.t. bregma, LM = 2.25 mm w.r.t. bregma, DV = -2.30 mm w.r.t the brain surface); in the same surgery, 250nl of helper virus mixture (AAV1-syn-F14F15S-sTpEptTA (diluted to 7.19E+10 GC/mL; Ai14 or Ai14 x TRE-CB mice) or AAV1-syn-FLEX-splitTVA-EGFP-tTA (diluted to 7.22E+10 GC/mL; Ai65F or Ai65F x TRE-CB mice) mixed with AAV1-TREtight-mTagBFP2-B19G (diluted to 6.50E+11) in a 50/50 ratio by volume) was injected into S1BF, layer 5 DLS projection region (AP = -1.55 mm w.r.t. bregma, LM = 3.00 mm w.r.t. bregma, DV = -0.75 mm w.r.t the brain surface). 7 days after AAV injection, 250nl of RVΔGL-Cre(EnvA) (6.13E+08 iu/ml) or RVΔGL-Flpo(EnvA) (7.67E+08 iu/ml, diluted to 6.13E+08 iu/ml) or RVΔG-Flpo(EnvA) (4.49E+09 iu/ml) or RVΔG-Cre (EnvA) (1.24E+10 iu/ml, diluted to 4.49E+09 iu/ml) was injected at the same cortical injection site as the helper viruses. For no-G controls, DPBS was included instead of AAV1-TREtight-mTagBFP2-B19G.

For longitudinal two-photon imaging for comparison of RVΔG -Flpo (B19G) and RVΔGL -Flpo (B10G), 200nL RVΔG-Flpo (B19G) (1.86E+10 iu/ml) or RVΔGL-Flpo(B19G) (1.86E+09 iu/ml) was injected into V1 (AP = -2.70 mm w.r.t. bregma, LM = 2.50 mm w.r.t. bregma, DV = -0.26 mm w.r.t. brain surface) into Ai65F mice. Glass windows composed of a 3mm-diameter glass coverslip (Warner Instruments CS-3R) glued (Optical Adhesive 61, Norland Products) to a 5mm-diameter glass coverslip (Warner Instruments CS-5R) were then affixed over the craniotomy with Metabond (Parkell), and custom stainless steel headplates (eMachineShop) were affixed to the skulls around the windows.

For longitudinal two-photon structural imaging of live monosynaptic tracing at the injection site, a 3 mm craniotomy was opened over primary visual cortex (V1). 300 nl of AAV1-syn-FLEX-splitTVA-EGFP-tTA (diluted to 7.22E+10 GC/mL; Ai65F or Ai65F x TRE-CB mice) mixed with AAV1-TREtight-mTagBFP2-B19G (diluted to 6.50E+11) in a 50/50 ratio by volume was injected into V1 (AP = -2.70 mm w.r.t bregma, LM = 2.50 mm w.r.t. bregma, DV = -0.26 mm w.r.t. brain surface), followed by implantation of windows as described above. Seven days after injection of helper AAVs, the coverslips were removed and 100 nl of RVΔGL-Flpo (EnvA) (7.67E+08 iu/mL) was injected at the same site. Coverslips were reapplied and custom stainless steel headplates (eMachineShop) were affixed to the skulls around the windows.

For functional imaging experiments, the V1 injection coordinates were AP = -2.45 mm w.r.t bregma, LM = 2.00 mm w.r.t bregma, DV = -0.26 mm w.r.t. brain surface, and the RVΔGL-Flpo(EnvA) (7.67E+08 iu/mL) was mixed in a 50/50 ratio by volume with AAV1-syn-F14F15S-jGCaMP7s (5.44E+12 GC/ml, diluted 1:10 in DPBS) before injection of 200 nl of the mixture 7d following the helper AAV injection.

Doxycycline administration

'No-dox' mice were fed with regular rodent chow throughout, while 'dox' mice were switched to chow containing doxycycline 200 mg/kg (Fisher Scientific, 14-727-450) beginning two weeks after RV injection and maintained on doxycycline chow until perfusion, in order to suppress rabies viral polymerase and glycoprotein expression. For the structural two-photon imaging experiment, 'dox' mice also received i.p. injections of 100 mg/kg doxycycline every 12 hours for three days, beginning two weeks after RV injection,

***In vivo* two-photon imaging and image analysis**

For longitudinal two-photon imaging of live monosynaptic tracing, injection sites were imaged on a Prairie/Bruker Ultima IV In Vivo two-photon microscope driven by a Spectra Physics Mai-Tai Deep See laser with a mode locked Ti:sapphire laser emitting at a wavelength of 1020 nm for tdTomato. Mice were reanesthetized and mounted via their headplates to a custom frame, with ointment applied to protect their eyes and with a handwarmer maintaining body temperature. One field of view was chosen in each mouse in the area of maximal fluorescent labelling. The imaging parameters were as follows: image size 1024 X 1024 pixels (565.1 µm x 565.1 µm), 0.360 Hz frame rate, dwell time 2.0 µs, 1x optical zoom, Z-stack step size 1 µm. Image acquisition was controlled with Prairie View 5.4 software. Laser power exiting the 20x water-immersion objective (Zeiss, W plan-apochromat, NA 1.0) varied between 20 and 65 mW depending on focal plane depth (Pockel cell value was automatically increased from 450 at the top section of each stack to 750 at the bottom section). For the example images of labeled cells, maximum intensity projections (stacks of 150-400 µm) were made with Fiji software. Cell counting was performed with the ImageJ Cell Counter plugin. When doing cell counting, week 1 tdTomato labelled cells were defined as a reference; remaining week 1 cells were the same cells at later time point that align with week 1 reference cells but the not-visible cells at week 1 (the dead cells). Plots of cell counts were made with Origin 7.0 software (OriginLab, Northampton, MA) or Prism 9 (GraphPad Software, San Diego, California).

For functional two-photon imaging of starting cells, injection sites in left-hemisphere V1 was chosen as the imaging area. This imaging was performed using the same microscope (5.356-Hz frame rate, 1024 X 128 pixels, 565.1 µm x 565.1 µm, dwell time 0.8 µs, 1x optical zoom, scan angle 45 degree) with the same objective and laser (at 920 nm) as in the structural imaging experiments. Laser power at the objective ranged from 10 to 65 mW. Calcium imaging data were acquired in supragranular layers (100 to 200 µm deep). Surface vasculature provided coarse fiducial markers for finding the same FOVs in subsequent weeks. Radial vasculature and cell body images from averaged data taken in the first session provided a template for fine alignment. The animal was awake, head-fixed and free to run on a circular disk. No behavioral training or reward was given. Visual stimuli were generated in Matlab (R2015R version) with custom software based on Psychtoolbox (http://psychtoolbox.org) and shown on the same LCD screen as in the widefield mapping experiments. Each condition consisted of 2 s of a full-field sine-wave grating drifting in one direction, presented at 80% contrast with spatial frequency of 0.04 cycles/ degree, followed by 2 s of uniform mean luminance (gray). All permutations of 12 directions (30° steps)

and 5 temporal frequencies (1, 2, 4, 8 and 15 Hz) were shown, in randomized order. The complete set was repeated 10 times, for a total stimulation period of 40 min per FOV per session. Cells were then manually segmented, and single-cell fluorescence traces were extracted by averaging the fluorescence of all pixels masking the soma. The mean ΔF/F over the full 2 s of each stimulus condition was used to calculate orientation tuning curves, with background fluorescence (F) in Δ F/F taken as the value of the trace immediately preceding a condition, averaged over all conditions. The raw calcium traces from cells within individual FOVs (not across FOVs, given different imaging conditions across animals and time points) were sorted by mean fluorescence.

Perfusions and histology

1 to 12 weeks (depending on experiment; see main text) after injection of rabies virus, mice were transcardially perfused with 4% paraformaldehyde in phosphate-buffered saline. Brains not used for two-photon imaging were postfixed overnight in 4% paraformaldehyde in PBS on a shaker at 4°C and cut into 50 µm coronal (S1 injections) or parasagittal (SNc injections) sections on a vibrating microtome (Leica, VT-1000S). Sections were collected sequentially into 6 tubes containing cryoprotectant, so that each tube contains a sixth of the collected tissue. For coronal sections, 15 rounds of section were collected. For sagittal sections, 12 rounds were collected. Brains from mice used for two-photon imaging were postfixed in 4% paraformaldehyde/30% sucrose in PBS for two days on a shaker at 4°C, then cut into 50 µm sections on a freezing microtome in a plane approximately tangential to the surface of the brain at the imaged location. Sections were immunostained as described[46] with the following primary antibodies (as applicable) at the following respective dilutions: chicken anti-GFP (Aves Labs GFP-1020) 1:500, guinea pig anti-parvalbumin (Synaptic Systems 195004) 1:1000, sheep anti-tyrosine hydroxylase (Millipore AB1542)) 1:1000, with secondary antibodies donkey anti-chicken Alexa Fluor 488 (Jackson Immuno 703-545-155) 1:200, donkey anti-guinea pig, AlexaFluor 647 conjugated (Jackson Immuno 706-605-148) 1:200, and donkey anti-sheep, AlexaFluor 647 conjugated (Jackson Immuno 713-605-147)) 1:200. Sections were mounted with Prolong Diamond Antifade mounting medium (Thermo Fisher P36970) and imaged on a confocal microscope (Zeiss, LSM 900).

Cell counts and statistical analysis

Labeled neurons in striatum (in DAT-IRES-Cre mice), contralateral cortex and thalamus (in PV-Cre mice and for the corticostriatal experiments), and at the injection sites were counted either manually or with the automated Cell Counter function in ImageJ, in every sixth 50 µm section on an epifluorescence microscope (Zeiss Imager.Z2). Coronal sections (corticostriatal experiments and PV-Cre) included sections between 1.2mm and -3.3mm relative to Bregma. Sagittal sections (DAT-IRES-Cre) covered sections 3.6mm to 0.0mm relative to Bregma. Cells expressing EGFP, mTagBFP2, or both, along with tdTomato, were counted by adding separate labels to each and then looking for overlapping cells. Groups were compared using single factor ANOVAs. Symbols denoting significance levels on graphs are as follows: *** = $p<0.001$; ** = $0.001 \leq p<0.01$; * = $0.01 \leq p<0.05$; n.s. = $p \geq 0.05$.

Reporting Summary

Further information on research design is available in the Nature Research Reporting Summary linked to this paper.

Data Availability

All cell counts and statistical analyses are provided in Supplementary Information. The novel plasmids described in this paper have been deposited with Addgene with the accession numbers given in Methods. The TRE-CB mouse line is being made available through the Jackson Laboratory (accession number 036974).

References

68. Turan, S., Kuehle, J., Schambach, A., Baum, C. & Bode, J. Multiplexing RMCE: versatile extensions of the Flp-recombinase-mediated cassette-exchange technology. *J Mol Biol* **402**, 52-69 (2010).
69. Dana, H. *et al.* High-performance calcium sensors for imaging activity in neuronal populations and microcompartments. *Nat Methods* **16**, 649-657 (2019).
70. Shimshek, D.R. *et al.* Enhanced odor discrimination and impaired olfactory memory by spatially controlled switch of AMPA receptors. *PLoS biology* **3**, e354 (2005).
71. Yusa, K., Zhou, L., Li, M.A., Bradley, A. & Craig, N.L. A hyperactive piggyBac transposase for mammalian applications. *Proc Natl Acad Sci U S A* **108**, 1531-6 (2011).

72. Matsuda, T. & Cepko, C.L. Electroporation and RNA interference in the rodent retina in vivo and in vitro. *Proceedings of the National Academy of Sciences of the United States of America* **101**, 16-22 (2004).
73. Gallardo, H.F., Tan, C. & Sadelain, M. The internal ribosomal entry site of the encephalomyocarditis virus enables reliable coexpression of two transgenes in human primary T lymphocytes. *Gene Ther* **4**, 1115-9 (1997).
74. Shaner, N.C. *et al.* Improved monomeric red, orange and yellow fluorescent proteins derived from Discosoma sp. red fluorescent protein. *Nature biotechnology* **22**, 1567-72 (2004).
75. Cetin, A.H. & Callaway, E.M. Optical Control of Retrogradely Infected Neurons Using Drug Regulated "TLoop" Lentiviral Vectors. *J Neurophysiol* (2014).
76. Krestel, H.E. *et al.* A genetic switch for epilepsy in adult mice. *The Journal of neuroscience : the official journal of the Society for Neuroscience* **24**, 10568-78 (2004).
77. Tallquist, M.D. & Soriano, P. Epiblast-restricted Cre expression in MORE mice: a tool to distinguish embryonic vs. extra-embryonic gene function. *Genesis* **26**, 113-5 (2000).
78. Kim, J.H. *et al.* High cleavage efficiency of a 2A peptide derived from porcine teschovirus-1 in human cell lines, zebrafish and mice. *PloS one* **6**, e18556 (2011).
79. Backman, C.M., Zhang, Y., Hoffer, B.J. & Tomac, A.C. Tetracycline-inducible expression systems for the generation of transgenic animals: a comparison of various inducible systems carried in a single vector. *J Neurosci Methods* **139**, 257-62 (2004).
80. Wickersham, I.R. *et al.* Lentiviral vectors for retrograde delivery of recombinases and transactivators. *Cold Spring Harb Protoc* **2015**, 368-74 (2015).
81. Wickersham, I.R., Sullivan, H.A. & Seung, H.S. Production of glycoprotein-deleted rabies viruses for monosynaptic tracing and high-level gene expression in neurons. *Nature protocols* **5**, 595-606 (2010).
82. Wickersham, I.R. & Sullivan, H.A. Rabies viral vectors for monosynaptic tracing and targeted transgene expression in neurons. *Cold Spring Harb Protoc* **2015**, 375-85 (2015).
83. Narayan, S., Barnard, R.J. & Young, J.A. Two retroviral entry pathways distinguished by lipid raft association of the viral receptor and differences in viral infectivity. *J Virol* **77**, 1977-83 (2003).

Acknowledgements

We thank Aurora Burds-Connor and Noranne Enzer of the Mouse ES Cell & Transgenic Facility at the Koch Institute for Integrative Cancer Research at MIT for generation of the TRE-CB line from ES cells. We thank Karel Svoboda for advice on titrating jGCaMP6s expression for reduced toxicity. We thank Xin Fu for his helpful observation on the design of the Flp-dependent helper AAV. Research reported in this publication was supported by BRAIN Initiative awards U01MH106018, U01MH114829, U19MH114830, and RF1MH120017 from the National Institute of Mental Health.

Author contributions

L.J. contributed molecular biology, cell culture, mouse colony management, virus injections, two-photon imaging, histology, microscopy, data analysis, and preparation of figures. H.A.S. produced viruses and conducted cell culture assays. M.Z. contributed perfusions, histology, microscopy, cell counts, data analysis, and mouse colony management. T.K.L. contributed virus injections, perfusions, histology, microscopy, and mouse colony management. M.M., C.X. and Y.H contributed cloning and molecular biology. N.E.L., M.P., & K.R.B. contributed mouse colony management, assisted with molecular biology. L.R. contributed cell counts. T.L.D. and H.Z. contributed embryonic stem cell targeting for making the TRE-CB mouse line. J.I., M.H., and M.S. assisted with establishing the structural and functional two-photon imaging. I.R.W. designed experiments and wrote the paper with input from L.J., H.A.S., M.Z., and other authors.

Competing interests

I.R.W. is a consultant for Monosynaptix, LLC, advising on design of neuroscientific experiments.

Additional information

Supplementary information is available for this paper.
A preprint version of this paper is available on bioRxiv.
Correspondence and requests for materials should be addressed to I.R.W. (wickersham@mit.edu).

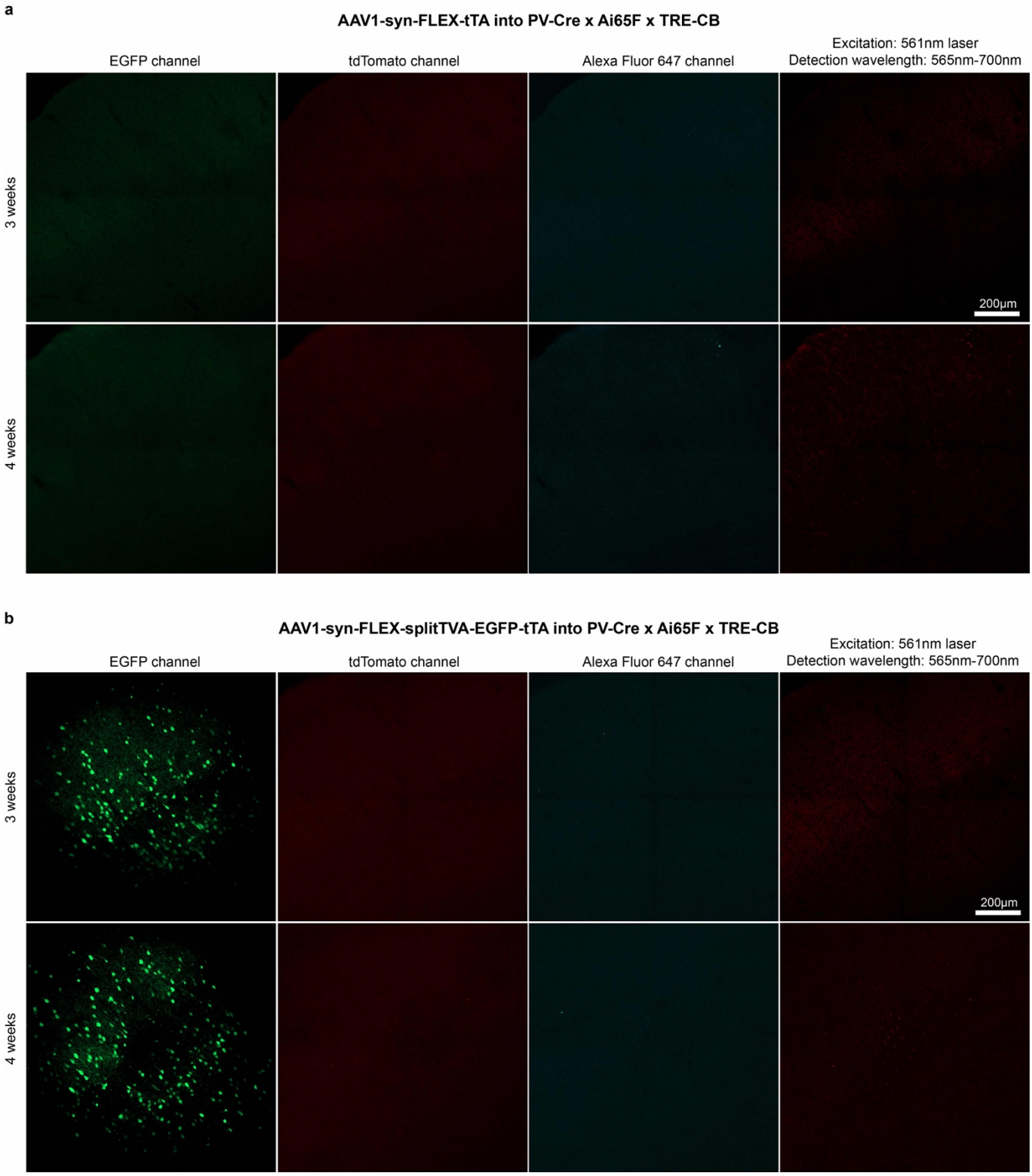

Extended Data Fig. 1: Intrinsic mCardinal fluorescence was not detected by confocal imaging, suggesting very low L expression in the conditions implemented. Representative confocal images of injection sites in PV-Cre x Ai65F x TRE-CB mice, showing lack of clear mCardinal fluorescence induced by either of the laser lines (561 nm or 640 nm) flanking the excitation maximum on the Zeiss LSM 900 confocal microscope. Because of the lack of fluorescence in the channel otherwise used for AlexaFluor 647, specifically, we were able to use that channel for immunostaining for PV and TH (Fig. 1 and Extended Data Figs. S2 & S3). **a,** Injection sites of a FLEX AAV expressing tTA without a fluorophore, and **b,** injection sites of the FLEX AAV expressing TVA, EGFP, and tTA, with survival times of 3 and 4 weeks in each case. Left: EGFP channel; center-left: tdTomato channel; center-right: AlexaFluor 647 channel; right: "best case" for imaging mCardinal: excitation with 561 nm and collecting all emitted light between 565 nm and 700 nm. Scale bars: 200 µm, apply to all panels.

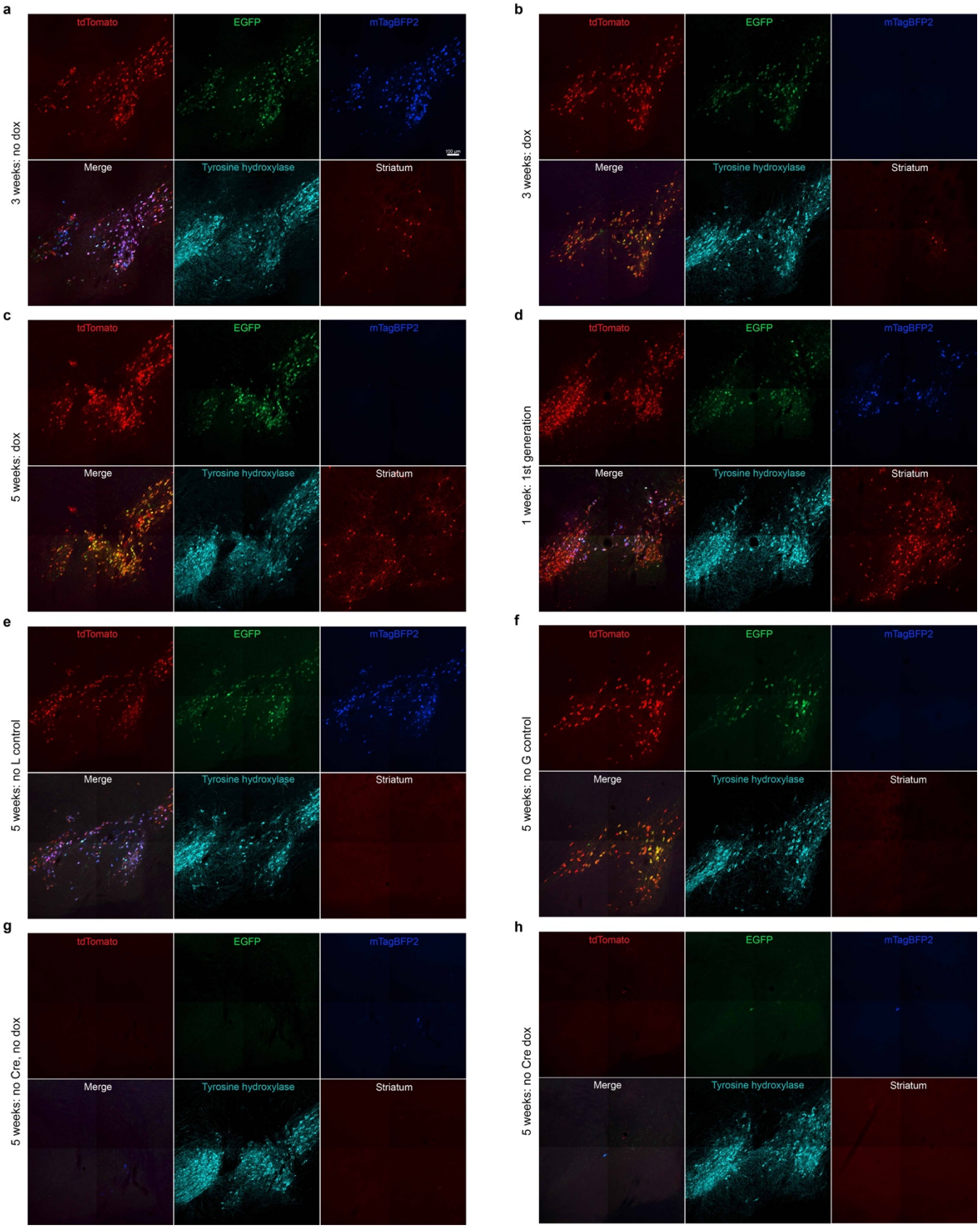

Extended Data Fig. 2: Representative images of second-generation monosynaptic tracing of inputs to dopaminergic midbrain neurons. See Fig. 1 for explanation of experimental design and for quantification. **a,** 3 weeks, no doxycycline, **b,** 3 weeks, with doxycycline, **c,** 5 weeks, with doxycycline. Control conditions shown here: **d,** first-generation (ΔG) system, **e,** no L, **f,** no G, **g,** no Cre, no doxycycline, **h,** no Cre, with doxycycline. Note that omitting L gave very similar results to omitting G.

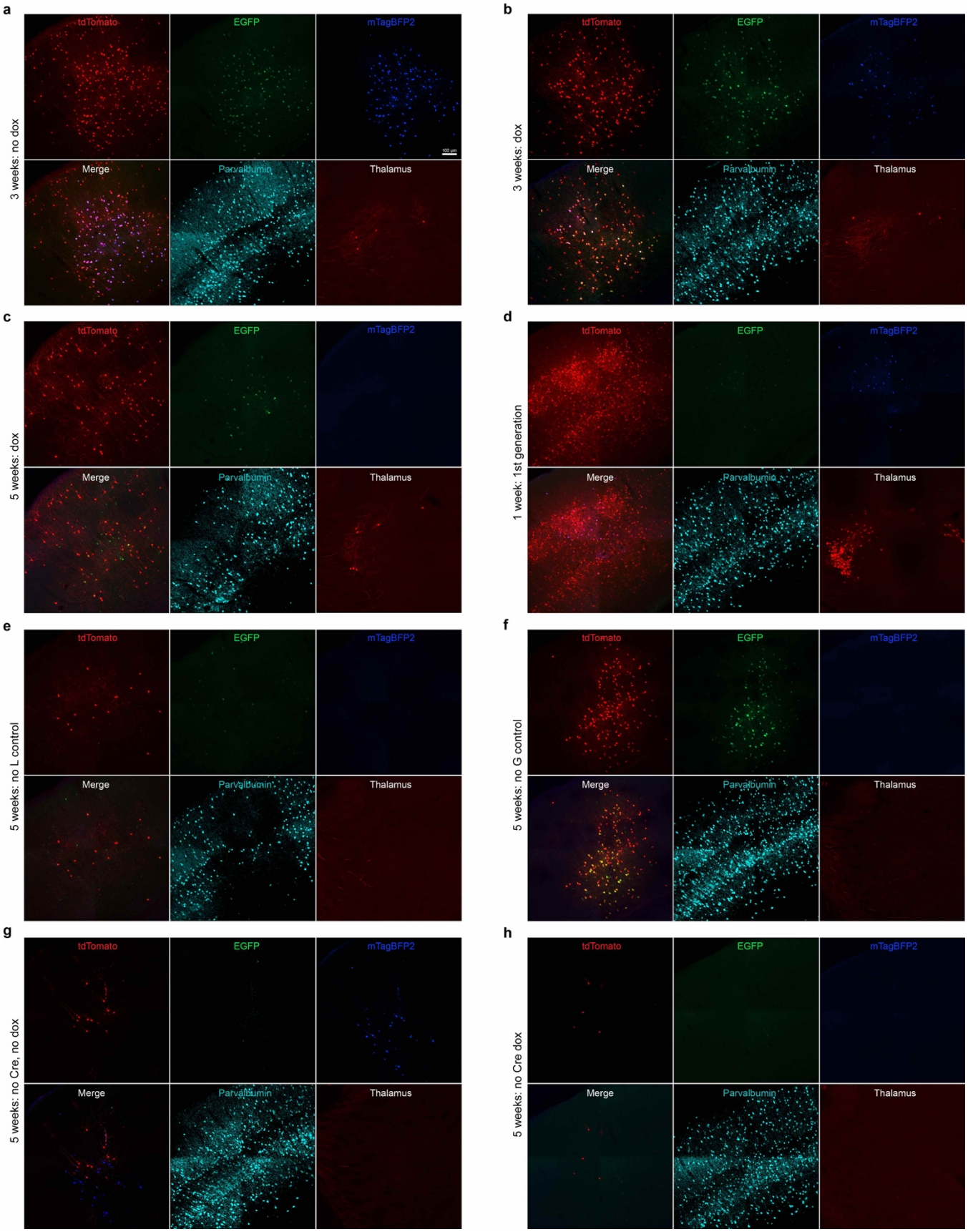

Extended Data Fig. 3: Representative images of second-generation monosynaptic tracing of inputs to parvalbumin-expressing cortical interneurons. See Fig. 1 for explanation of experimental design and for quantification. **a,** 3 weeks, no doxycycline, **b,** 3 weeks, with doxycycline (note that there is still blue fluorescence in this image, suggesting that, at one week after the mice were switched to dox food, the doxycycline has not completely suppressed G and presumably L expression), **c,** 5 weeks, with

doxycycline. Control conditions shown here: d) first-generation (ΔG) system, e) no L, f) no G, g) no Cre, no doxycycline, h) no Cre, with doxycycline. Again, omitting L and omitting G gave very similar results.

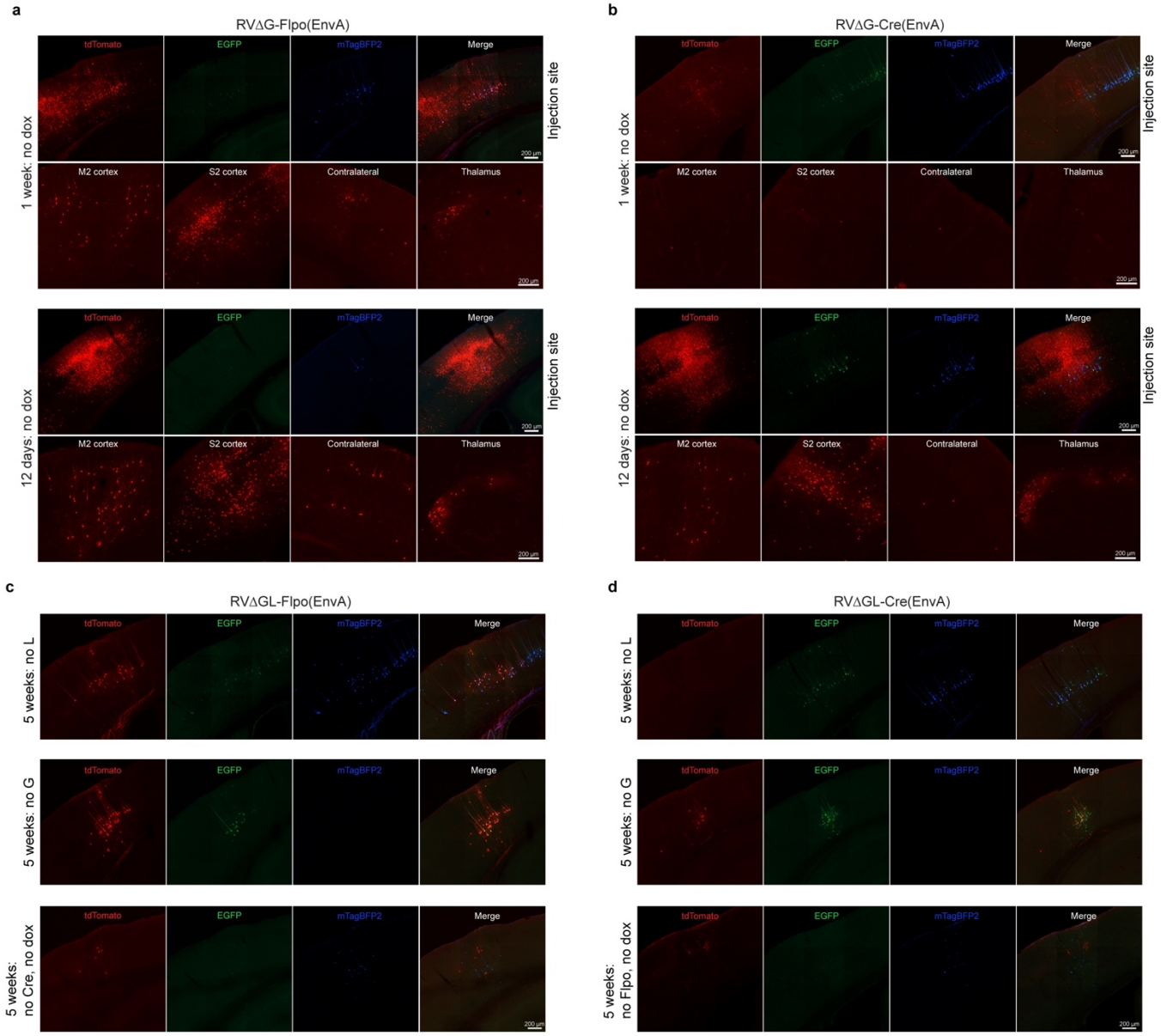

Extended Data Fig. 4: Representative images of control experiments for corticostriatal experiments. See Fig. 2 for explanation of experimental design and quantification. **a-b,** First-generation controls (7d and 12d survival times). **c-d,** no L, no G, and no Cre/Flpo controls (all without doxycycline). Scale bars: 200 µm, apply to all images.

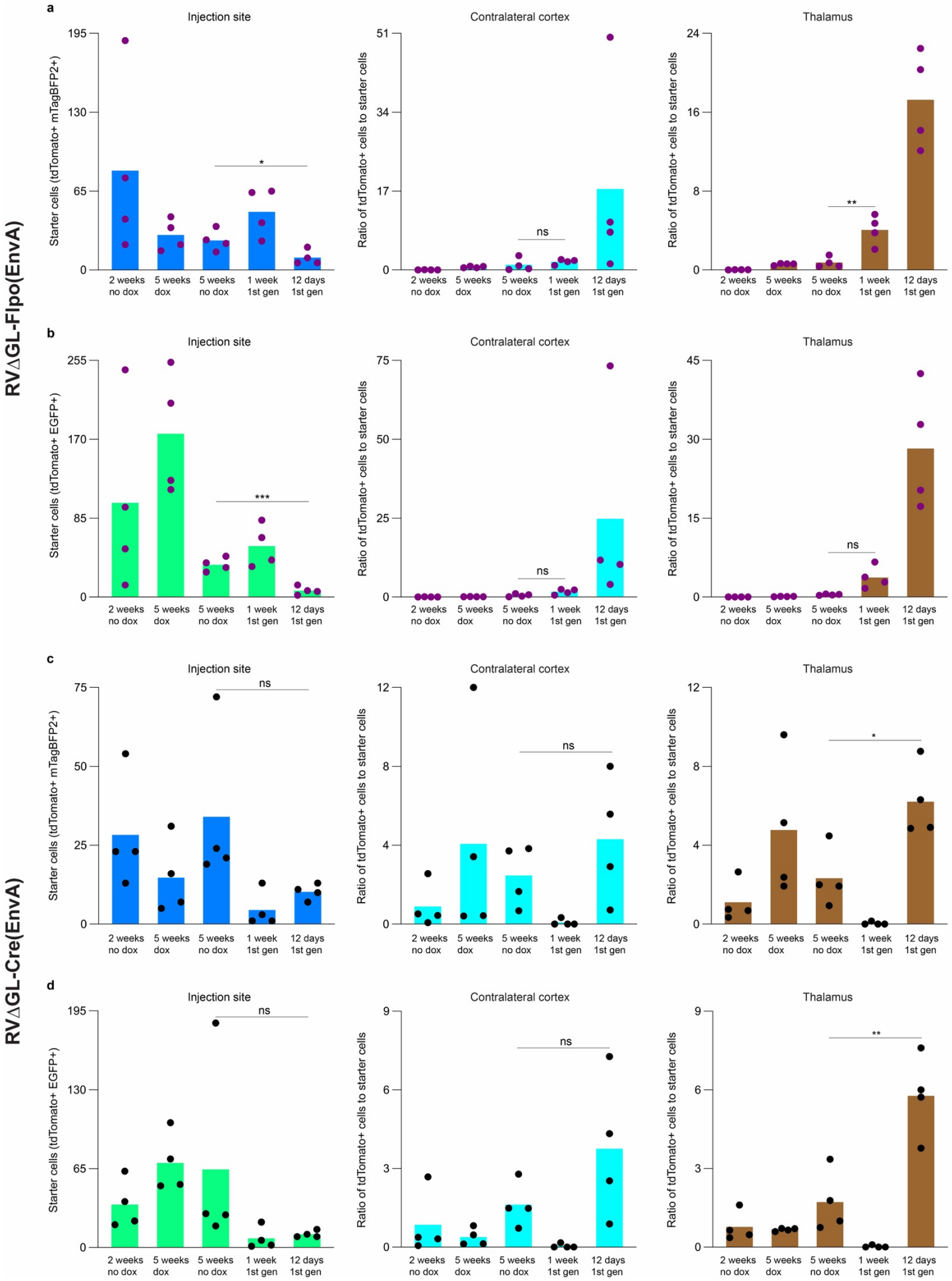
RVΔGL-Flpo(EnvA)
RVΔGL-Cre(EnvA)
a
b
c
d
Injection site
Contralateral cortex
Thalamus
Starter cells (tdTomato+ mTagBFP2+)
Starter cells (tdTomato+ EGFP+)
Ratio of tdTomato+ cells to starter cells
2 weeks no dox
5 weeks dox
5 weeks no dox
1 week 1st gen
12 days 1st gen
*
**
***
ns

Extended Data Fig. 5: Counts of corticothalamic "starting cells" and ratios of contralateral and thalamic cells to starting cells. a-b, Results using RV∆GL-Flpo(EnvA). **a,** Counts of starting cells (left), defined here as cells coexpressing tdTomato (marking activity of Flpo) and mTagBFP2 (marking expression of G), and ratios of these numbers of starting cells to numbers of tdTomato+ cells in contralateral cortex (middle) and thalamus (right). **b,** Counts and ratios of starting cells, defined here as cells coexpressing tdTomato (marking activity of Flpo) and EGFP (marking expression of TVA and tTA). **c-d,** Results using RV∆GL-Cre(EnvA). **c,** Counts and ratios of starting cells, defined here as cells coexpressing tdTomato (marking activity of Cre) and mTagBFP2 (marking expression of G). **d,** Counts and ratios of starting cells, defined here as cells coexpressing tdTomato (marking activity of Cre) and EGFP (marking expression of TVA and tTA).

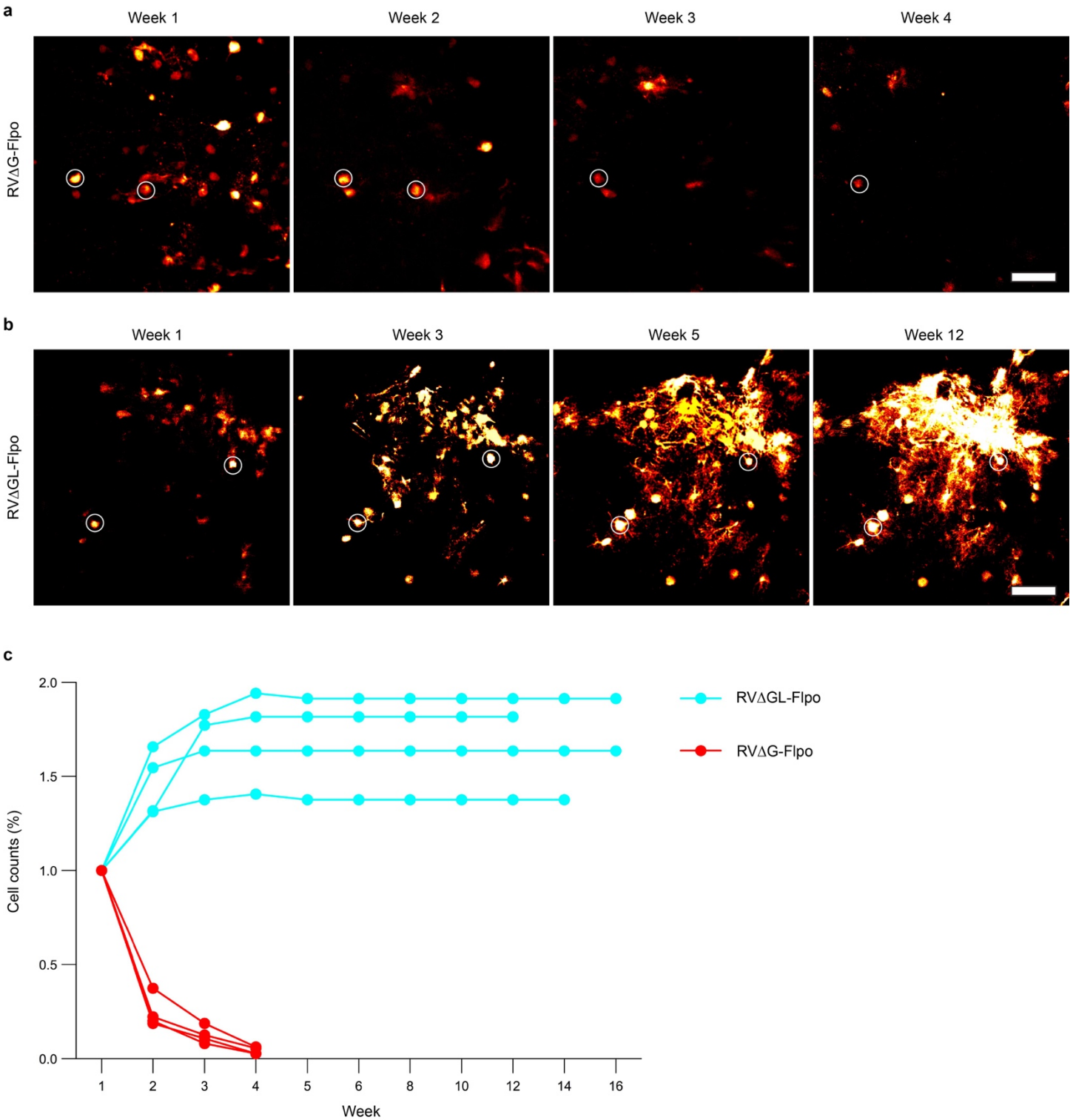

Extended Data Fig. 6: Second-generation rabies virus encoding Flpo is nontoxic to labeled neurons. a, Representative images of longitudinal two-photon structural imaging fields of view (FOVs) from one week (left) to 4 weeks (right) after injection of a first-generation rabies viral vector encoding Flpo (RVΔG-Flpo). The viruses in this experiment were coated with the native RV glycoprotein for direct (TVA-independent) infection of neurons. Images are of the same FOV at different time points. This first-generation virus killed almost all infected cells in this FOV within 4 weeks: only two labeled cells (circled) survived until the 4-week timepoint. Scale bar: 100 μm. **b,** Representative images of longitudinal two-photon structural imaging FOVs from one week (left) to 12 weeks (right) after injection of a second-generation rabies viral vector encoding Flpo (RVΔGL-Flpo). Images are of the same FOV at different time points. All labeled cells are still present at 16 weeks, the last timepoint of imaging. Two example labeled cells are circled as fiducial markers. Scale bar: 100 μm. **c,** Fraction of visible labeled

cells over time, relative to the number visible at one week after RVΔG-Flpo or RVΔGL-Flpo injection; connected sets of dots represent counts obtained from the same FOV within the same mouse at the different time points (for RVΔG-Flpo: 1 week to 4 weeks; for RVΔGL-Flpo: 1 week to 16 weeks). Cells infected by RVΔG-Flpo (red) have almost entirely disappeared by 4 weeks postinjection. The number of cells labeled by RVΔGL-Flpo (cyan) increases up to 4 weeks postinfection and then remains constant for as long as the brains were imaged.

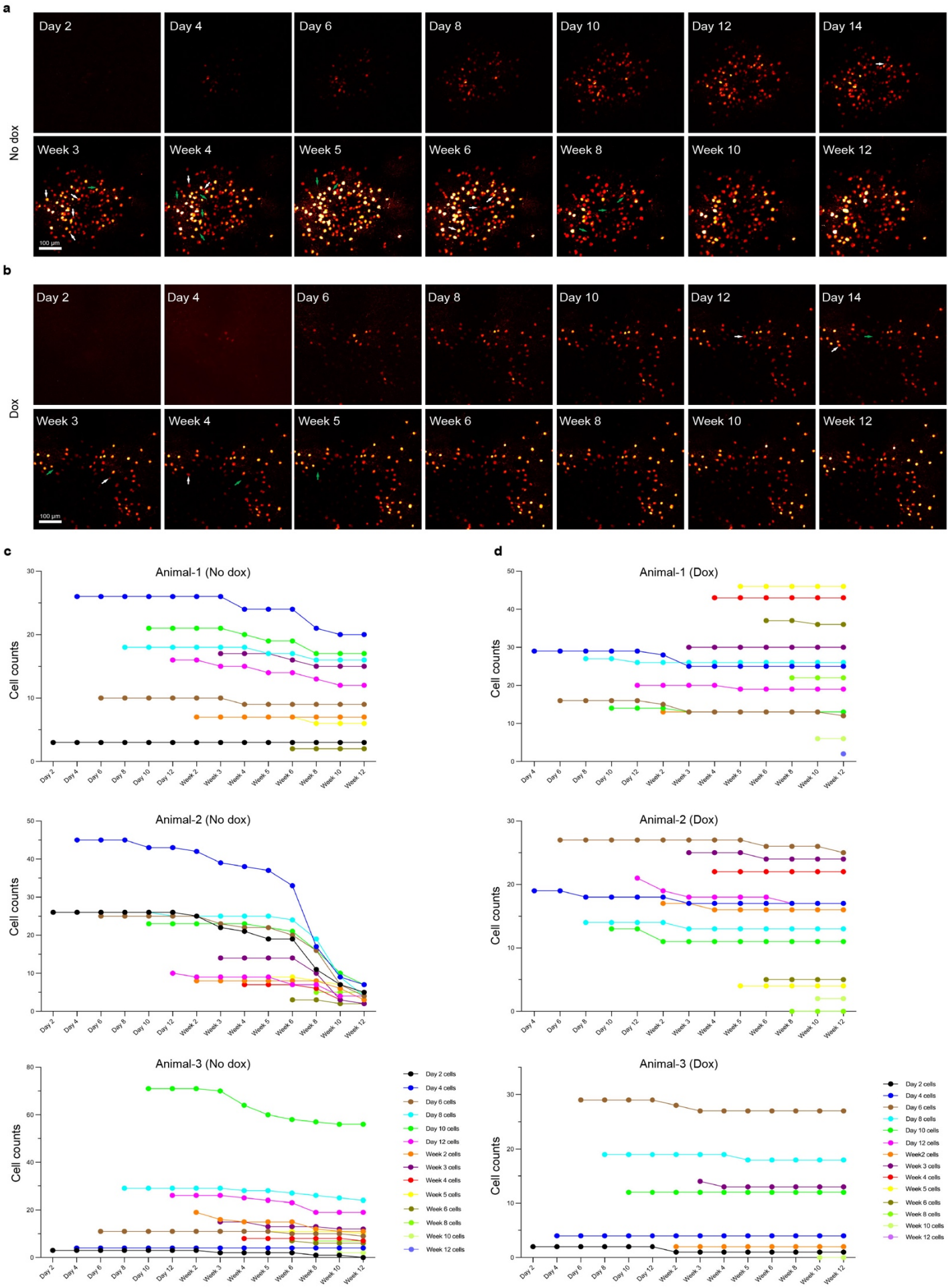
a
No dox
Day 2
Day 4
Day 6
Day 8
Day 10
Day 12
Day 14
Week 3
Week 4
Week 5
Week 6
Week 8
Week 10
Week 12
100 µm
b
Dox
c
Animal-1 (No dox)
Animal-2 (No dox)
Animal-3 (No dox)
Cell counts
d
Animal-1 (Dox)
Animal-2 (Dox)
Animal-3 (Dox)
Day 2 cells
Day 4 cells
Day 6 cells
Day 8 cells
Day 10 cells
Day 12 cells
Week 2 cells
Week 3 cells
Week 4 cells
Week 5 cells
Week 6 cells
Week 8 cells
Week 10 cells
Week 12 cells

Extended Data Fig. 7: Additional examples of longitudinal two-photon imaging of second-generation monosynaptic tracing *in vivo*. a-b, Example images of tdTomato-labelled neurons at the injection site in V1 over all imaging sessions, from 2 days to 12 weeks, in two mice. The 'No dox' mice (**a**) were fed with regular food throughout, while the 'Dox' mice (**b**) were fed with food containing doxycycline (200 mg/kg) starting at two weeks after RV injection until perfusion at week 12, in order to suppress expression of the rabies virus polymerase and glycoprotein genes. White arrows show example cells that are last seen at that time point, with green arrows indicating the former positions of those now-missing cells at the next time point. In these examples, a total of 20 out of 141 cells were lost in the 'No dox' mouse, whereas 5 out of 98 cells were lost in the 'Dox' mouse. Scale bar: 100 μm. **c-d,** Counts of tdTomato-labeled cells appearing at each timepoint in individual mice. Each connected set of dots represents the numbers of the cells that appeared at one timepoint that are still present at the subsequent timepoints.

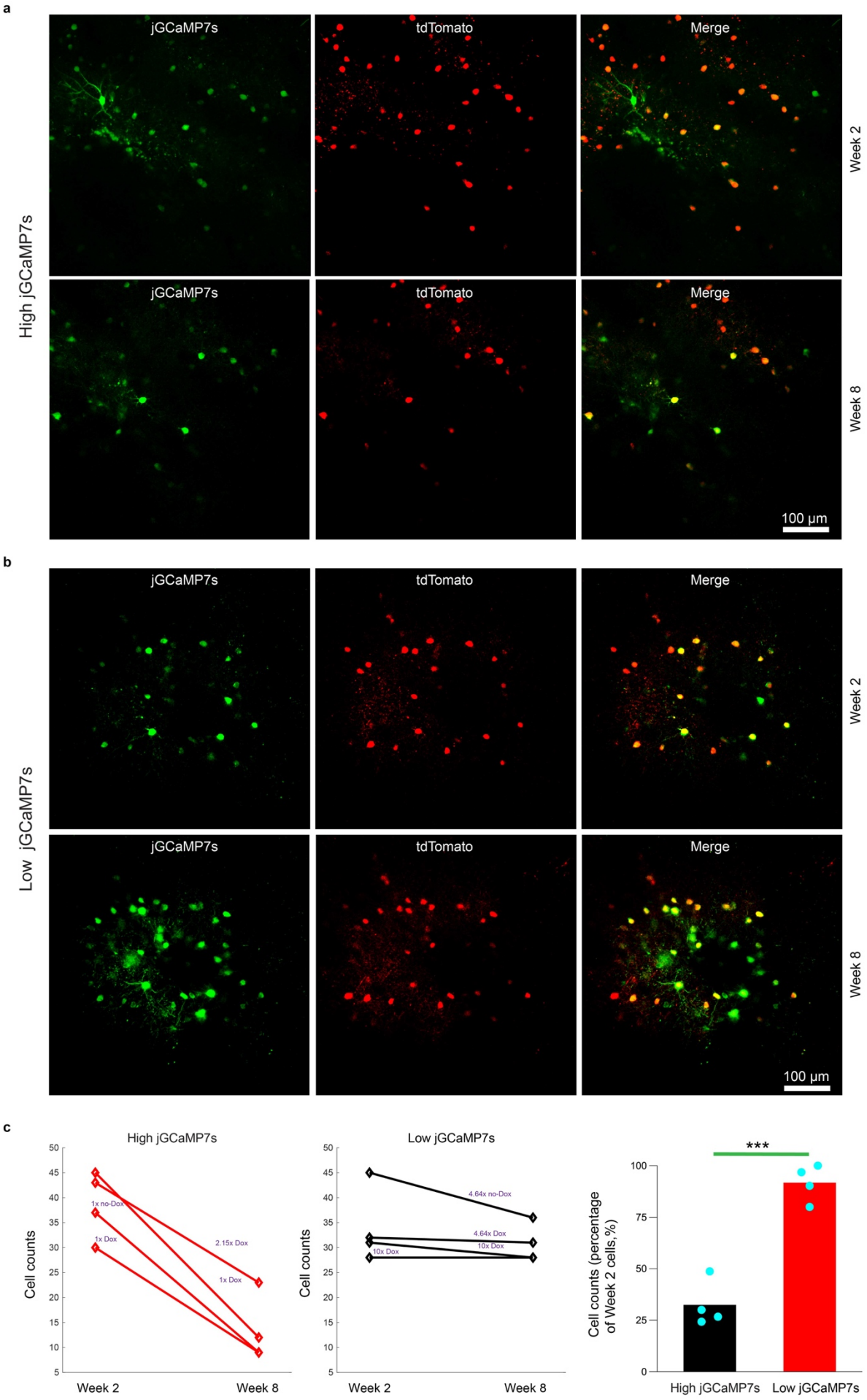
a
jGCaMP7s
tdTomato
Merge
Week 2
High jGCaMP7s
jGCaMP7s
tdTomato
Merge
Week 8
100 µm
b
jGCaMP7s
tdTomato
Merge
Week 2
Low jGCaMP7s
jGCaMP7s
tdTomato
Merge
Week 8
100 µm
c
High jGCaMP7s
Cell counts
1x no-Dox
1x Dox
2.15x Dox
1x Dox
Week 2
Week 8
Low jGCaMP7s
Cell counts
4.64x no-Dox
4.64x Dox
10x Dox
10x Dox
Week 2
Week 8
***
Cell counts (percentage of Week 2 cells, %)
High jGCaMP7s
Low jGCaMP7s

Extended Data Fig. 8: Titration of jGCaMP7s AAV concentration to minimize toxicity from jGCaMP7s overexpression. a, Representative two-photon images of neurons expressing tdTomato and jGCaMP7s, with the Flp-dependent AAV1 expressing jGCaMP7s injected at a higher concentration (2.15x diluted from maximum), with doxycycline administered. Top row: 2 weeks after injection. Bottom row: the same FOV at 8 weeks after injection. Numerous cells visible at 2 weeks are no longer seen at 8 weeks. Scale bar: 100 um. **b,** Representative two-photon images from another mouse, in which the Flp-dependent AAV1 expressing jGCaMP7s had been injected at a lower concentration (4.64x diluted from maximum), with doxycycline administered. Top row: 2 weeks after injection. Bottom row: the same FOV at 8 weeks after injection. Almost all cells seen at 2 weeks are still present at 8 weeks. Scale bar: 100 μm. **c,** Counts of jGCaMP7s- and tdTomato-expressing neurons infected with high-concentration (left graph) and low-concentration (middle graph) jGCaMP7s AAV. Each data point was obtained from one FOV from each animal. Virus dilution factor and doxycycline condition are marked on the top of each line; for example, '10x, Dox' means the mouse received the 10-fold dilution of jGCaMP7s AAV and doxycycline food two weeks after the second injection. The surviving cell percentage is shown in the right graph; there is a significant decrease in the high concentration of jGCaMP7s group (***$p=0.00036<0.001$, one-way ANOVA test).

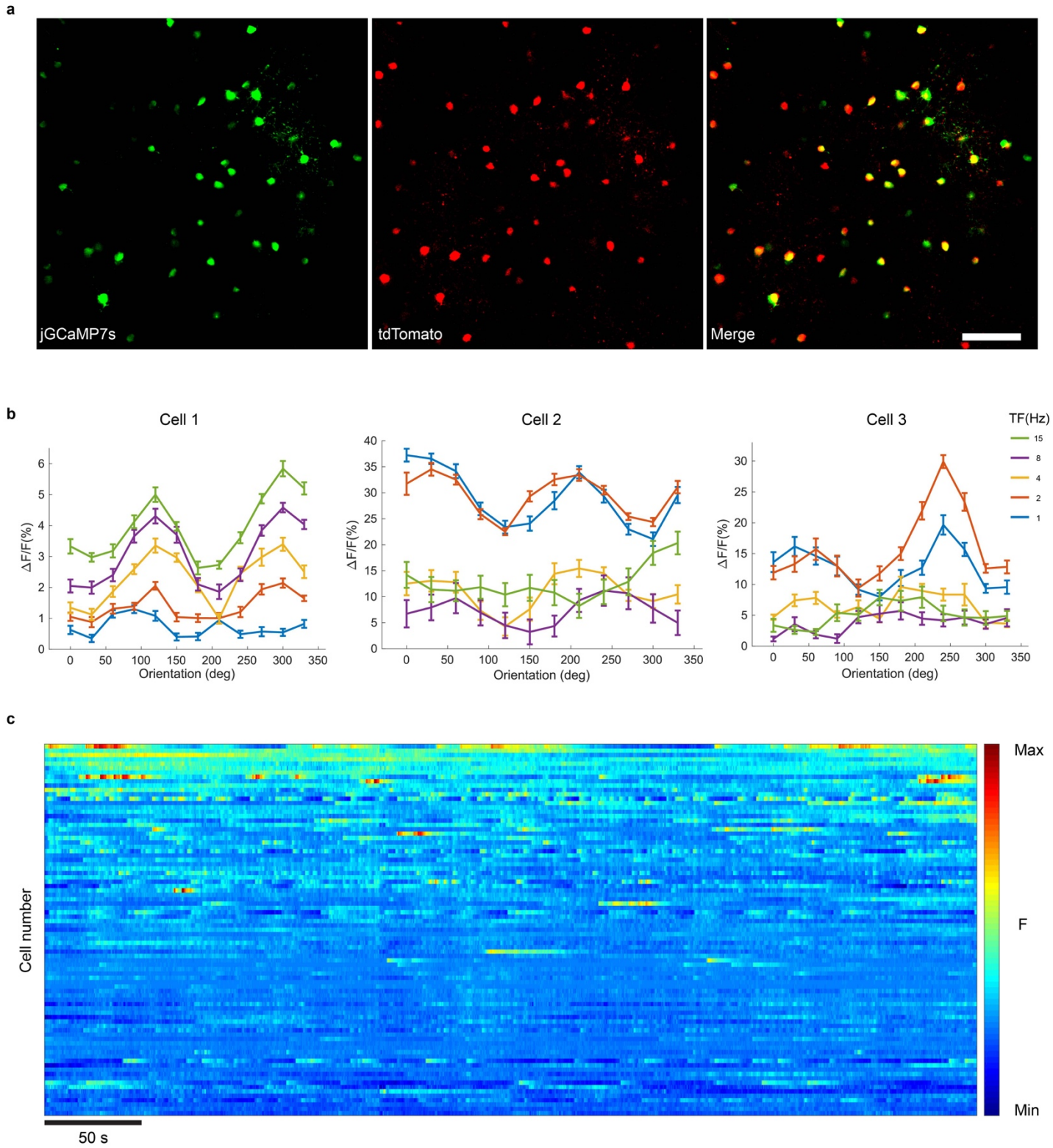

Extended Data Fig. 9: Additional examples of two-photon functional imaging of labeled cells in mouse visual cortex. a, Representative two-photon images of neurons expressing jGCaMP7s and tdTomato at 3 weeks. Scale bar: 100 μm. **b,** Direction tuning curves of three different jGCaMP7s-expressing neurons obtained with drifting gratings presented at 12 directions of motion and 5 temporal frequencies (TF), repeated 10 times (mean ΔF/F ± s.e.m.) at 8 weeks; color coding and axis labels are as in Fig. 4. **c,** Single-cell fluorescence time courses for 85 cells over the first 480 s of visual stimulation, showing robust spontaneous and evoked activity. Scale bar: 50 s.

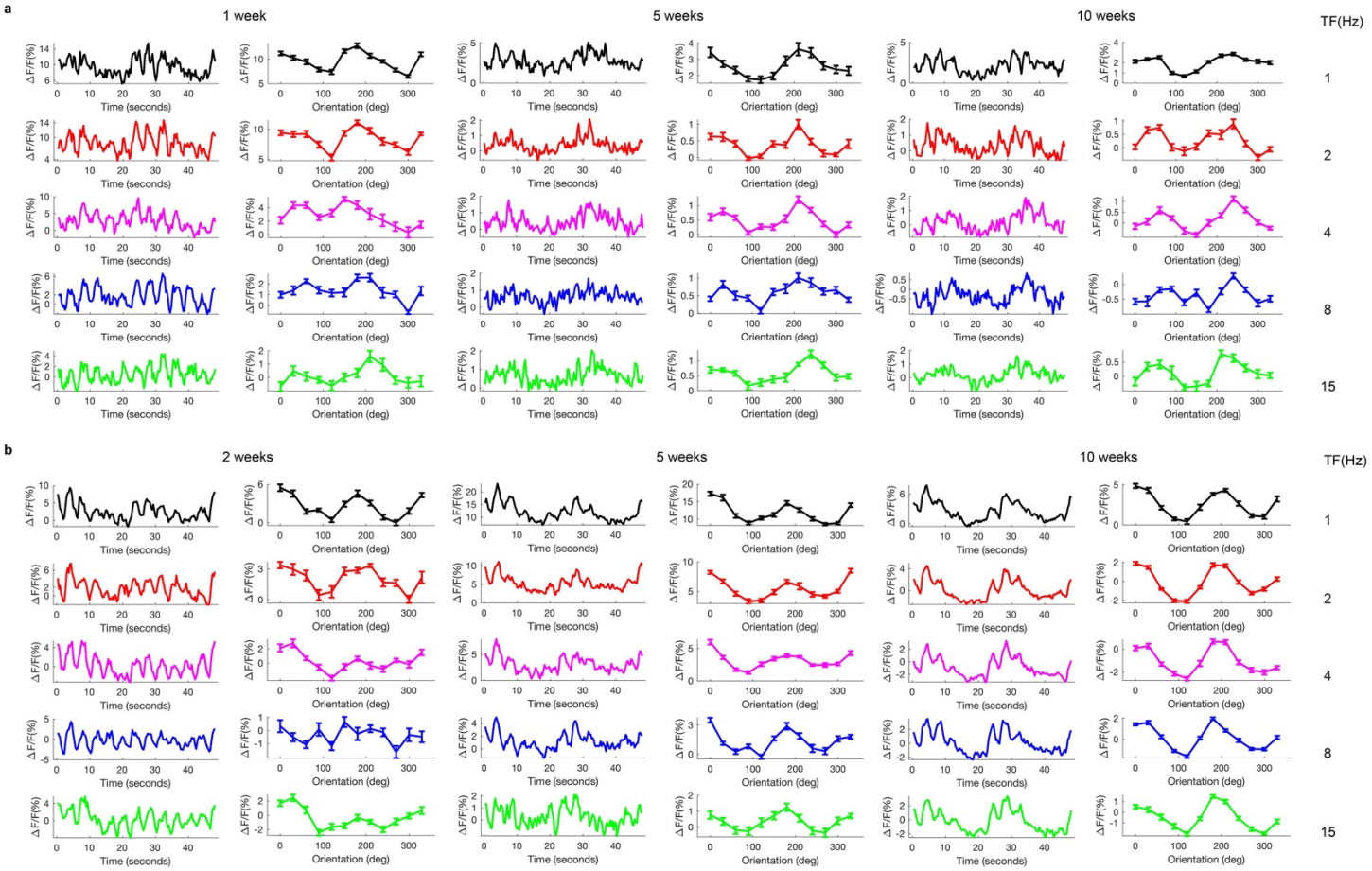

Extended Data Fig. 10: jGCaMP7s signals and tuning curves of two example V1 neurons over multiple imaging sessions. a, jGCaMP7s signals and tuning curves of a "week 1" cell (i.e., in which jGCaMP7s and tdTomato fluorescence could be detected seven days after RVΔGL-Flpo(EnvA) and AAV1-syn-F14F15S-jGCaMP7s injection). These data were obtained with drifting gratings presented at 12 directions of motion and 5 temporal frequencies (TF), repeated 10 times (tuning curve: mean ΔF/F ± s.e.m; jGCaMP7s signals: mean ΔF/F) in three different imaging sessions (left: week 1; middle: week 5; right: week 10). **b,** jGCaMP7s signals and tuning curves of a "week 2" cell (the same cell as used for Fig. 4d).

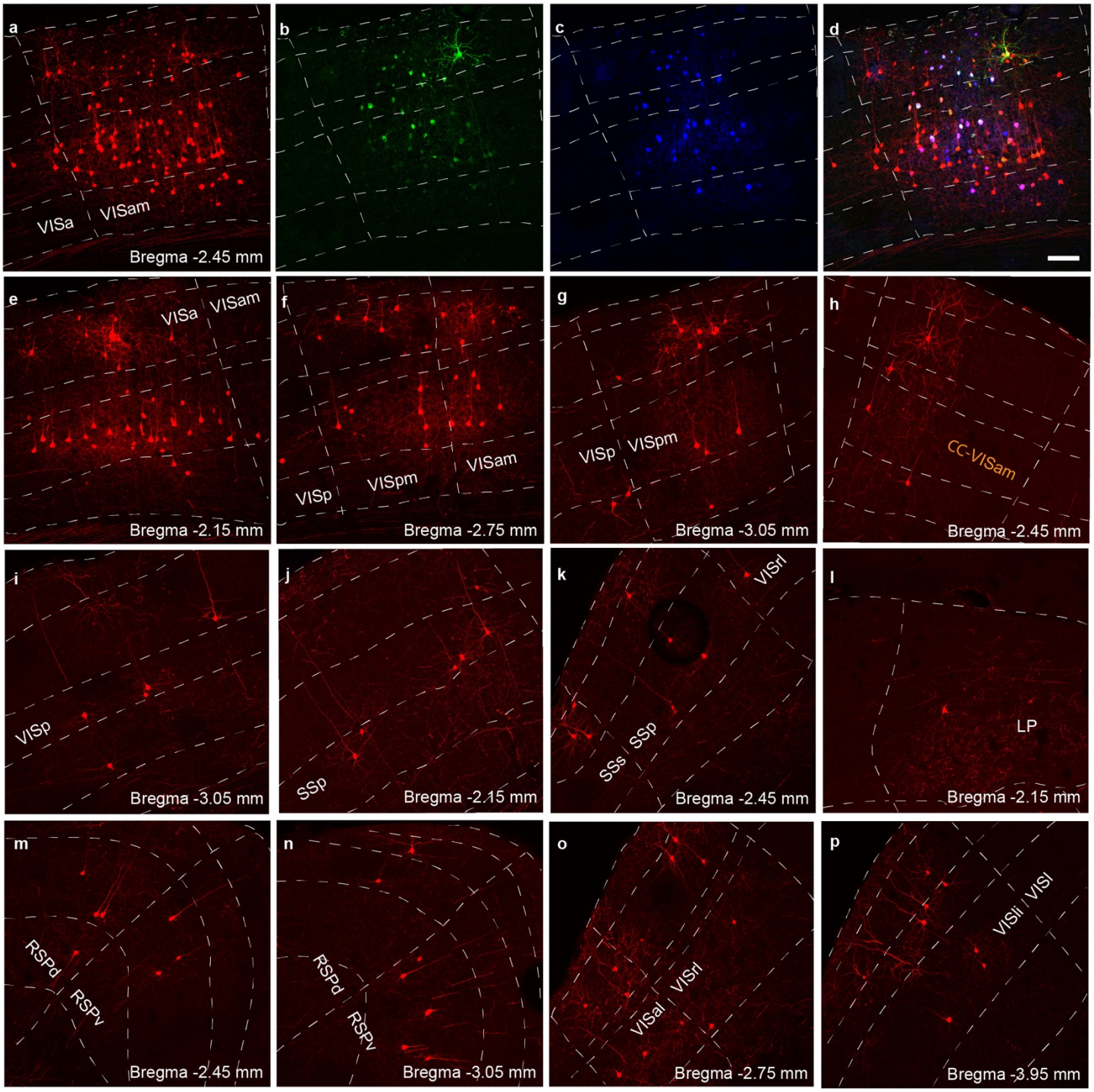

Extended Data Fig. 11: Example confocal images of injection site and input regions in mouse used for longitudinal functional calcium imaging. See Fig. 4a for diagram of experimental design. These images show that inclusion of the jGCaMP7s AAV did not prevent successful monosynaptic tracing. **a-d,** Injection site in V1. **a,** tdTomato, **b),** jCaMP7s, **c,** mTagBFP2, **d,** merge. Scale bar: 100 µm, applies to all panels. **e-p,** Inputs to parvalbumin-expressing V1 neurons are found in many different brain regions: other visual areas (**e-g**, **i**, **o-p**), contralateral cortex (**h**), somatosensory areas (**j-k**), thalamus (**l**), and retrosplenial areas (**m-n**). VISa, anterior visual area; VISam, anteromedial visual area; VISp: Primary visual area; VISpm: Posteromedial visual area; CC-VISam: Contralateral cortex - Anteromedial visual area; SSs: Supplemental somatosensory area; SSp: Primary somatosensory area; LP: Lateral posterior nucleus of the thalamus; RSPd: Retrosplenial area, dorsal part; RSPv: Retrosplenial area, ventral part; VISal: Anterolateral visual area; VISrl: Rostrolateral visual area; VISli: Laterointermediate visual area; VISl: Lateral visual area.

BD FACSDiva 8.0

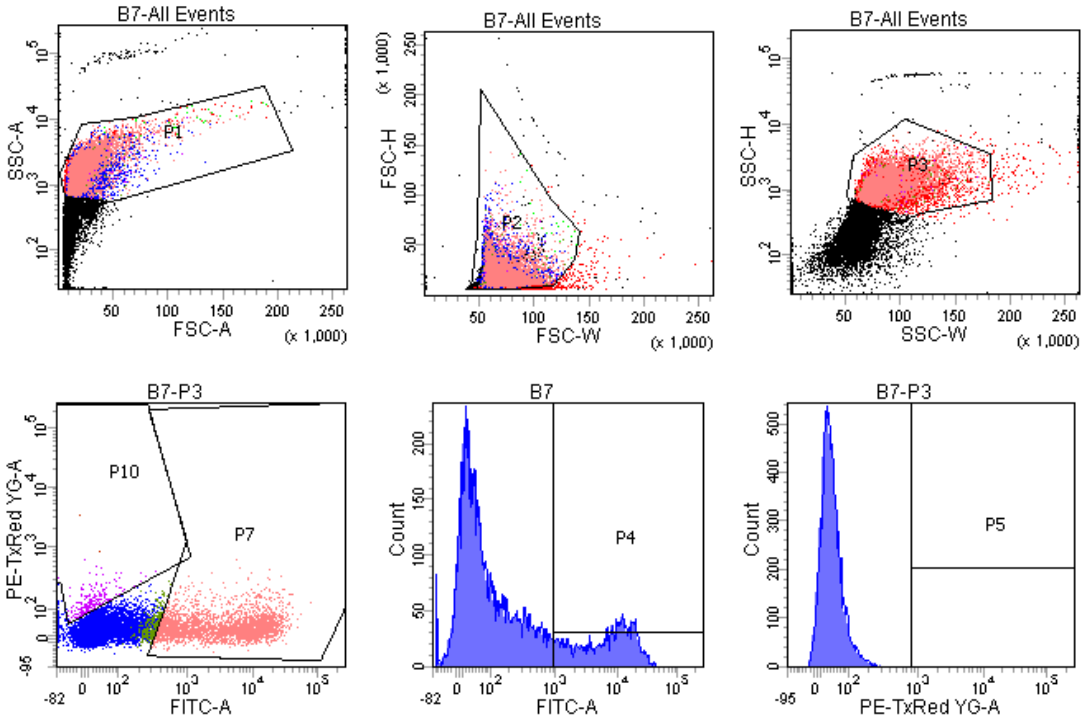

Experiment Name:	2020-11-24_dGL-4Cre and-4Fl...
Specimen Name:	RVdGL-4Flpo(EnvA)_III conc
Well Name:	B7
Record Date:	Nov 24, 2020 1:07:31 PM
$OP:	HeatherSullivan
GUID:	345bd03b-03fe-4027-b2f6-2b3...

Population	%Parent	FITC-A Mean	Pacific Blu... Mean	PE-TxRed ... Mean
P4	22.7	9,013	21	41
P10	2.1	17	14	172
P6	0.0	####	####	####
P8	0.0	-20	124	3,393
P5	0.0	6	68	2,116
P9	33.0	6,338	18	40
P7	30.4	6,871	20	39
P11	0.0	6	68	2,116

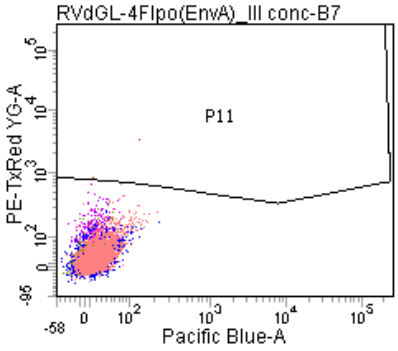

Population	#Events	%Parent	%Total
All Events	20,739	####	100.0
P1	11,313	54.5	54.5
P2	10,064	89.0	48.5
P3	10,000	99.4	48.2
P4	2,266	22.7	10.9
P5	2	0.0	0.0
P6	0	0.0	0.0
P8	1	0.0	0.0
P9	3,304	33.0	15.9
P1	214	2.1	1.0
P7	3,036	30.4	14.6
P1	2	0.0	0.0

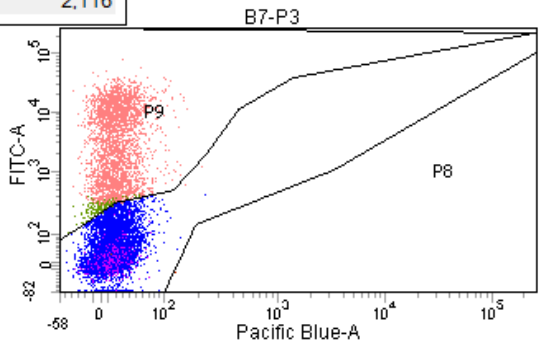

Extended Data Fig. 12: Representative example of FACS data for titering viruses. This example, included as stipulated by the Nature Portfolio Reporting Summary, shows FACS analysis data for one

dilution of RV∆GL-Flpo(EnvA), used to infect HEK 293T cells which were immunostained for the rabies virus nucleoprotein using a blend of FITC-conjugated monoclonal antibodies (see Methods). The middle histogram in the second row shows the characteristic bimodal distribution (less distinct with second-generation RV vectors than with first-generation ones) with the uninfected cells in the mode on the left and infected ones in the one on the right. Gates are set by comparison with negative control wells of uninfected cells.

Supplementary File 1: Counts and statistics for DAT-IRES-Cre experiments.

Supplementary File 2: Counts and statistics for PV-Cre experiments.

Supplementary File 3: Counts and statistics for corticostriatal experiments.

Supplementary File 4: Counts and calculations for estimation of starting cell survival rates.